Final Report • November 1990

EVALUATION OF A DIFFUSION/TRAPPING MODEL FOR HYDROGEN INGRESS IN HIGH-STRENGTH ALLOYS

AD-A229 288

Bruce G. Pound, Senior Electrochemist
Materials Research Laboratory

DTIC
ELECTE
NOV 27 1990
S   D
D

SRI Project PYU 1962

Prepared for:

Department of the Navy
Office of Naval Research
800 N. Quincy Street
Arlington, VA 22217

Attn: Dr. A. J. Sedriks

Contract No. N00014-86-C-0233

Approved:

D. D. Macdonald, Laboratory Director
Materials Research Laboratory

G. R. Abrahamson
Senior Vice President
Sciences Group

REPORT DOCUMENTATION PAGE

1a. REPORT SECURITY CLASSIFICATION	1b. RESTRICTIVE MARKINGS
Unclassified	

2a. SECURITY CLASSIFICATION AUTHORITY	3 DISTRIBUTION / AVAILABILITY OF REPORT
	Approved for public release – distribution unlimited.
2b. DECLASSIFICATION / DOWNGRADING SCHEDULE	

4. PERFORMING ORGANIZATION REPORT NUMBER(S)	5. MONITORING ORGANIZATION REPORT NUMBER(S)
PYU-1962	

6a. NAME OF PERFORMING ORGANIZATION	6b. OFFICE SYMBOL (If applicable)	7a. NAME OF MONITORING ORGANIZATION
SRI International		

6c. ADDRESS (City, State, and ZIP Code)	7b. ADDRESS (City, State, and ZIP Code)
333 Ravenswood Ave Menlo Park, CA 94025-3493	

8a. NAME OF FUNDING / SPONSORING ORGANIZATION	8b OFFICE SYMBOL (If applicable)	9. PROCUREMENT INSTRUMENT IDENTIFICATION NUMBER
Office of Naval Research	1131I	N00014-86-C-0233

8c. ADDRESS (City, State, and ZIP Code)	10. SOURCE OF FUNDING NUMBERS			
800 N. Quincy St Arlington, VA 22217-5000	PROGRAM ELEMENT NO.	PROJECT NO	TASK NO.	WORK UNIT ACCESSION NO

11 TITLE (Include Security Classification)

Evaluation of a Diffusion/Trapping Model for Hydrogen Ingress in High Strength Alloys
(Unclassified)

12. PERSONAL AUTHOR(S)
Bruce G. Pound

13a. TYPE OF REPORT	13b. TIME COVERED	14. DATE OF REPORT (Year, Month, Day)	15. PAGE COUNT
Final Technical	FROM 8811 TO 9011	901114	100

16. SUPPLEMENTARY NOTATION

17.	COSATI CODES		18. SUBJECT TERMS (Continue on reverse if necessary and identify by block number)
FIELD	GROUP	SUB-GROUP	Inconel 625, Hastelloy C-276, Hydrogen Ingress,
			Inconel 718, 18Ni Maraging Steel Hydrogen Trapping,
			Incoloy 925, Titanium, Trapping Model

19. ABSTRACT (Continue on reverse if necessary and identify by block number)

Structural heterogeneities in alloys are potential traps for hydrogen. Identifying the dominant types of traps is crucial to determining the susceptibility of an alloy to hydrogen embrittlement. The objective of this research was to obtain the hydrogen ingress and trapping characteristics for a range of microstructures and so identify the dominant type of irreversible trap in different alloys. A diffusion/trapping model was used in conjunction with a potentiostatic pulse technique to study the ingress of hydrogen in three precipitation-hardened alloys (Inconel 718, Incoloy 925, and 18Ni maraging steel), two work-hardened alloys (Inconel 625 and Hastelloy C-276), titanium (pure and grade 2), and copper-enriched AISI 4340 steel in 1 mol/L acetic acid-1 mol/L sodium acetate containing 15 ppm arsenic oxide. In all cases except pure titanium, the data were shown to fit the interface-control form of the model and values were determined for the irreversible trapping constants (k) and the flux of hydrogen into the alloys. The density of irreversible trap defects were calculated from k and generally found to be in close

20. DISTRIBUTION / AVAILABILITY OF ABSTRACT	21. ABSTRACT SECURITY CLASSIFICATION
☒ UNCLASSIFIED/UNLIMITED ☐ SAME AS RPT. ☐ DTIC USERS	Unclassified

22a. NAME OF RESPONSIBLE INDIVIDUAL	22b. TELEPHONE (Include Area Code)	22c. OFFICE SYMBOL
A. J. Sedriks	(202) 696-4402	1131I

DD FORM 1473, 84 MAR   83 APR edition may be used until exhausted.
All other editions are obsolete.

agreement with the concentration of a specific heterogeneity in each alloy. Moreover, the trapping constants for the alloys were found to be consistent with their relative susceptibilities to hydrogen embrittlement.

ACKNOWLEDGMENTS

DTIC
COPY
INSPECTED
6

Accesion For	
NTIS CRA&I	☑
DTIC TAB	☐
Unannounced	☐
Justification	
By	
Distribution /	
Availability Codes	
Dist	Avail a 'd / or Special
A-1	

CONTENTS

ILLUSTRATIONS

TABLES

INTRODUCTION

Hydrogen embrittlement can restrict the use of various metals and alloys in aqueous environments. The degradation of mechanical properties as a result of hydrogen ingress is of particular concern in high-strength alloys. Local interactions between the hydrogen and heterogeneities in the microstructure initiate the series of events leading to failure. Accordingly, a knowledge of the hydrogen interaction with heterogeneities in different alloys contributes to an understanding of the susceptibility of high-strength alloys to hydrogen embrittlement.

The structural heterogeneities in alloys are potential trapping sites for diffusing hydrogen, and the nature of the interaction of hydrogen with these trap sites affects the resistance of the alloy to hydrogen embrittlement. Traps with both a high binding energy and a high specific saturability (maximum number of hydrogen atoms that can be trapped per defect) for hydrogen are thought to be the most conducive to hydrogen embrittlement.[1-3] The accumulation of hydrogen at second-phase particles and precipitates is generally considered to promote microvoid initiation via the fracture of particles or the weakening of particle-matrix interfaces. In contrast, metals containing a high density of well-distributed strong traps (high binding energy) that have a low specific saturability should show little susceptibility to embrittlement. Therefore, identifying the dominant types of traps is crucial to determining the susceptibility of an alloy to hydrogen embrittlement.

The objective of this research was to obtain the hydrogen ingress and trapping characteristics for a range of microstructures and so identify the dominant type of irreversible trap in different alloys. A model for the diffusion and trapping of hydrogen atoms was used in conjunction with a potentiostatic pulse technique to provide information on the trapping behavior that is not directly available from other methods.[4] The pulse technique and diffusion/trapping model have previously been applied to iron,[5] a high-strength steel (AISI 4340), and two high-strength nickel-base alloys (Monel K-500 and MP35N).[6]

In this work, we extended the application of the technique and model to four groups of other alloys: (1) precipitation-hardened nickel-containing alloys (Inconel 718, Incoloy 925, and 18Ni maraging steel), (2) cold-worked nickel-base alloys (Inconel 625 and Hastelloy C-276), (3) titanium (pure and grade 2), and (4) copper-enriched high-strength

1

steel (AISI 4340). Data obtained by applying the model were used to compare the trapping capability of the individual alloys and thereby provide a basis for explaining differences in the resistance of these alloys to hydrogen embrittlement.

The composition of each alloy was provided by the manufacturer and is given in Tables 1 and 2. The titanium specimen was 99.99% pure.

Table 1
ALLOY COMPOSITION (wt %)

Element	Alloy				Steel		Titanium
	718	925	C-276	625	18NI	4340[a]	Grade 2
Al	0.60	0.30		0.18	0.13	0.031	
B	0.003				0.003		
C	0.03	0.02	0.002	0.03	0.009	0.42	0.021
Co	0.16		0.83		9.15		
Cr	18.97	22.20	15.27	22.06	0.06	0.89	
Cu	0.04	1.93			0.11	0.19	
Fe	16.25	28.96	5.84	4.37	balance	balance	0.17
Mn	0.10	0.62	0.48	0.17	0.01	0.46	
Mo	3.04	2.74	16.04	8.70	4.82	0.21	
N						0.005	0.007
O						0.001	0.16
Nb+Ta	5.30			3.50			
Ni	54.41	40.95	57.5	60.33	18.42	1.74	
P	0.009		<0.005	0.012	0.004	0.009	
S	0.002	0.001	<0.002	0.001	0.001	0.001	
Si	0.11	0.17	<0.02	0.38	0.04	0.28	
Ti	0.98	2.11		0.27	0.65		balance
W			3.90		0.01		
Other			0.12 V		0.05 Ca 0.02 Zr		<0.0050 H

[a] As received.

All the materials were supplied in the form of rod with a diameter of 1.27 cm. The precipitation-hardened alloys were used as received, whereas the Inconel 625 and Hastelloy were cold-worked 17 and 27%, respectively, to obtain their final yield strengths. 4340 steel, heat-treated to yield strengths of 1206 and 1792 MPa, has been studied in previous work, and only a high Cu (0.7%) form of 4340 steel (designated as high-Cu 4340 steel) was examined in the current tests. The Cu-steel was prepared by arc-melting copper granules with the as-received steel under argon, and the hardness of the resulting alloy was 47, corresponding to a yield strength of approximately 1496 MPa. The yield strength and the particle characteristics of each alloy as used, and of 4340 steel for comparison, are given in Table 2.

Table 2
CHARACTERISTICS OF ALLOYS

Alloy	Heat Treatment[a]	Yield Strength (MPa)	Particle Characteristics		
			Type	d_c (µm)	Concentration (m^{-3})
718	Hot finish, solution treated	1238	NbTi(CN)	7.8	2.2×10^{13}
925	Hot finish, annealed, aged	758	TiC	2.9	4.1×10^{13}
625	Hot finish , annealed	1195	NbTi(C)	2.5	7.4×10^{13}
C-276	Hot rolled	1237	-	-	-
18Ni Steel	Aged (482°C, 4 hr)	1954	TiC/Ti(CN)	3.4	1.1×10^{13}
Ti Grade 2	Annealed (620°C, 1 hr)	380	-	-	-
4340 Steel[b]	Annealed	1792	MnS	18.4	2×10^9
Cu-Steel	-	1496	n[c]	-	-

[a] Provided by manufacturer
[b] Heat-treated[6]
[c] n = not examined

All the nickel-containing alloys except the Hastelloy develop micrometer-sized MC-type carbides (where M is the metallic component). In the case of Inconel 718, the carbide has been identified as niobium carbide with some titanium and titanium nitride dissolved in it or NbTi(CN),[7] and Inconel 625 is known to form MC-type carbides that are rich in Nb.[8]

4

Large MC carbide particles have also been identified in Incoloy 901,[9] which is similar in titanium content to the 925 alloy, and maraging steels can form carbides and carbo-nitrides, Ti(CN).[10,11] All the specimens used in this study were found to contain large particles randomly distributed, and an energy dispersive X-ray (EDX) analysis showed the particles to contain titanium, with niobium also present in Inconels 625 and 718. Scanning electron micrographs of Hastelloy C-276 showed one or two submicron spots that were assumed to be particles but were too small to identify by EDX, and it was concluded that there were a negligible number, if any, carbide-type particles in the C-276 alloy.

The characteristic dimension (d_c) of these particles was determined as the mean of the linear dimensions in the exposed plane. The concentration of particles was calculated on the basis of a spherical shape, with the radius taken as half the characteristic dimension. In the case of the maraging steel, there was a considerable distribution in the particle size and some degree of uncertainty in the particle concentration.

Details of the electrochemical cell and instrumentation have been given previously.[6] The test electrodes of each alloy consisted of a 5-cm length of rod press-fitted into a Teflon sheath so that only the planar end surface was exposed to the electrolyte. The surface was polished with SiC paper followed by 0.05-μm alumina powder. The same sample of each alloy was used throughout the study, but it was repolished before each experiment to remove metal previously exposed to absorbed hydrogen. The electrolyte was an acetate buffer (1 mol L^{-1} acetic acid/1 mol L^{-1} sodium acetate) containing 15 ppm As$_2$O$_3$ as a hydrogen entry promoter. The electrolyte was deaerated with argon for 1 hr before measurements began and throughout data acquisition. The potentials were measured with respect to a saturated calomel electrode (SCE). All tests were performed at $22 \pm 2°$C.

The pulse technique has been described previously.[4-6] Briefly, the test electrode is charged with hydrogen at a constant potential (E_c) for a time (t_c), after which the potential is stepped to a more positive value, E_A (10 mV negative of the open-circuit potential). The charging time was varied from 0.5 to 50 s for each E_c. Anodic current transients with a charge (q_a) were obtained for each charging time over a range of overpotentials ($\eta = E_c - E_{oc}$). The open-circuit potential (E_{oc}) of the test electrode was sampled immediately before each charging time and was also used to monitor the stability of the surface film; film reduction was evident from a progressive shift of E_{oc} to more negative values with each t_c at a sufficiently high charging potential.

The presence of the surface oxide can in principal affect the data analysis because the diffusion/trapping model implicitly assumes that the oxide thickness constitutes an

5

insignificant fraction of the total diffusion distance traversed by the mobile hydrogen. The composition and thickness of the passive film on three high-nickel alloys (Inconel 718, Incoloy 925, and MP35N) were investigated using surface analysis by laser ionization (SALI). Details of this study are described in the Appendix. The film thickness was found to be similar for the three alloys and estimated to be 1.5 ± 0.5 nm, whereas the depth of hydrogen penetration in the alloys ranges from 0.14 to 0.32 μm for charging times from 10 to 50 s. Hence, the films represent only about 0.5-1% of the total diffusion distance in the high nickel alloys and are thin enough that they represent a negligible fraction of the overall diffusion distance traversed by hydrogen during charging times of 10 s and longer.

ANALYSIS

DIFFUSION/TRAPPING MODEL

Typical anodic current transients for a nickel-containing alloy (Inconel 718) and titanium (grade 2) are shown in Figures 1 and 2. The diffusion/trapping model used to analyze the anodic transients has been developed for two cases under conditions imposed by the pulse technique: (1) diffusion control, in which the rate of hydrogen ingress is controlled by diffusion in the bulk metal; and (2) interface control, in which the rate of ingress is controlled by the flux across the interface.[4] Analysis of the transients assuming diffusion control gave trapping parameters that changed with t_c and E_c, indicating that this limiting case was not appropriate to any of the alloys studied.

The data were therefore analyzed in terms of the interface control model, for which the total charge passed out is given in nondimensional form[4] by

$$Q'(\infty) = \sqrt{R}\{1 - e^{-R}/\sqrt{(\pi R)} - [1 - 1/(2R)]\text{erf}\sqrt{R}\} \tag{1}$$

The nondimensional terms are defined by $Q = q/[FJ\sqrt{(t_c/k_a)}]$ and $R = k_a t_c$, where q is the dimensionalized charge in C cm^{-2}, F is the Faraday constant, and J is the ingress flux in mol cm^{-2} s^{-1}. The charge $q'(\infty)$ corresponding to $Q'(\infty)$ is equated to q_a. k_a is an apparent trapping constant measured for irreversible traps in the presence of reversible traps and is given by $k/(1 + K_r)$, where k is the irreversible trapping constant and K_r is an equilibrium constant for reversible traps.

The adsorbed charge (q_{ads}) was found to be negligible in all cases, and so q_a was assumed to be associated entirely with absorbed hydrogen. Data for q_a could be fitted to Eq. (1) to obtain values of k_a and J such that the ingress flux was constant over the range of charging times and k_a was essentially independent of charging potential. As discussed previously,[6] the data analysis was restricted to charging times ≥ 10 s.

7
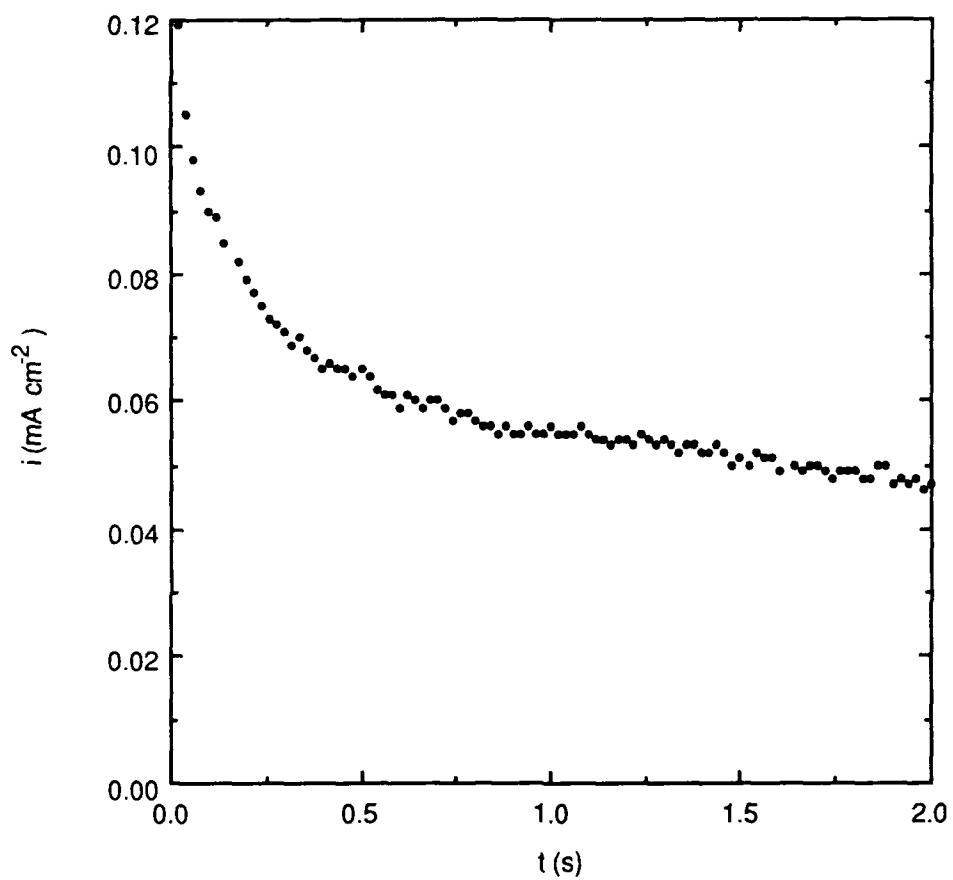
RA-1962-19

Figure 1. Anodic transient for Inconel 718 in acetate buffer.
$t_c = 10$ s; $E_c = -0.671$ V (SCE).

The full transient is not shown.

8
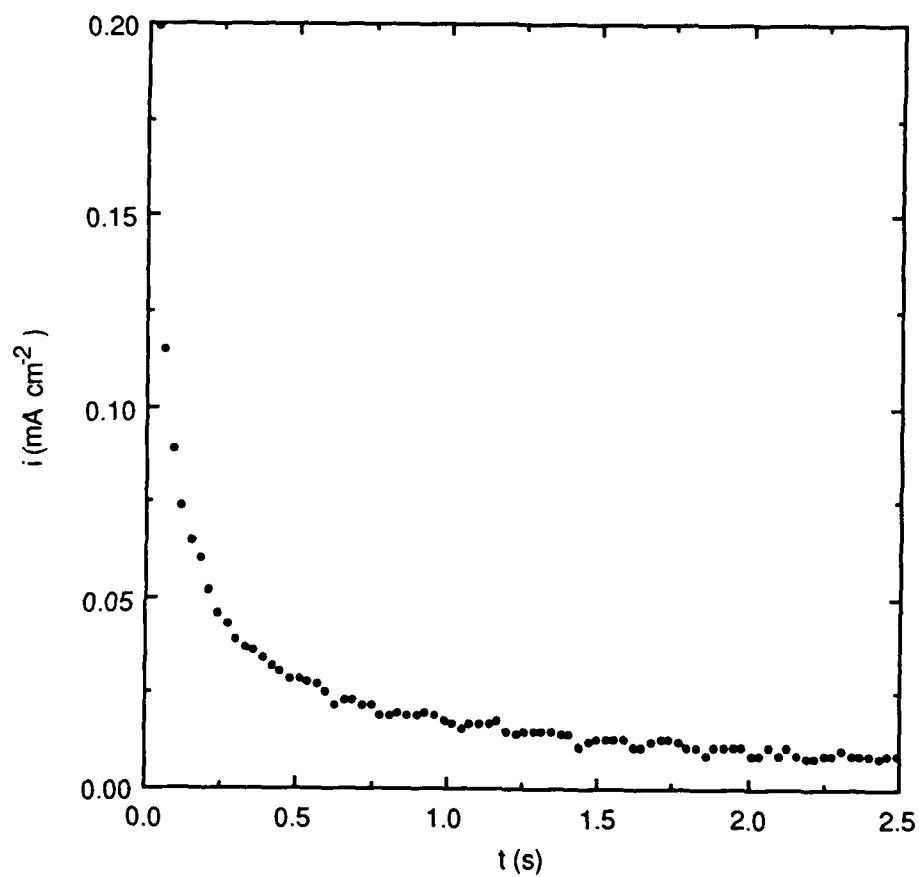
Figure 2. Anodic transient for titanium grade 2 in acetate buffer.
$t_c = 15$ s; $E_c = -0.742$ V (SCE).

The full transient is not shown.

9

The values of k_a and J can be used to calculate the irreversibly trapped charge (q_T) given nondimensionally by

$$Q_T = [\sqrt{R} - 1/(2\sqrt{R})]\text{erf}\sqrt{R} + e^{-R}/\sqrt{\pi} \qquad (2)$$

The charge associated with the entry of hydrogen into the metal (q_{in}) can be determined from its nondimensional form of $Q_{in} = \sqrt{R}$ by using the derived value of k_a. The data for q_{in}, q_T, and the cathodic charge (q_c) can then be used to obtain two ratios: (1) q_T/q_{in}, corresponding to the fraction of hydrogen in the metal that is trapped; and (2) q_{in}/q_c, representing the fraction of charge associated with hydrogen entry during the charging step. The ratio q_T/q_{in} is independent of potential because each component has the same dependence on flux, whereas q_{in}/q_c generally shows some variation with potential.

EVALUATION OF TRAP DENSITY

The density of irreversible traps (N_i) can be obtained from the trapping constant (k) on the basis of a knowledge of the dimensions of the potential traps and the hydrogen diffusivity. The trapping constant can be used to calculate the density of irreversible trap particles by using a model based on spherical traps of radius d:[5]

$$k = 4\pi d^2 N_i D_L/a \qquad (3)$$

where D_L is the lattice diffusivity of hydrogen and a is the diameter of the metal atom. The apparent diffusivity (D_a) is given by $D_L/(1 + K_r)$,[6] so the irreversible trapping constant (k) can be expressed as $k_a D_L/D_a$. Therefore, the trap density can be represented in terms of the apparent trapping constant:

$$N_i = k_a a/(4\pi d^2 D_a) \qquad (4)$$

Although the apparent diffusivity is needed to calculate N_i, the diffusivity (D_L) for the trap-free "pure" metal or alloy is not required. The calculation of N_i also involves the trap radius (d), and the evaluation of d presupposes a knowledge of potential irreversible traps. Thus, in calculating N_i from k_a, the microstructure of the alloy must be characterized in terms of the dimensions of its heterogeneities. The dominant irreversible trap can then be

10

identified by comparing the trap density with the concentrations of potential traps in the alloy.

The assumption of spherical traps in the above model is an approximation in most cases, and models for specific trap geometries may lead to more accurate values of the trap density. In alloys where the concentrations of potential traps have distinct ranges, the incorporation of a more applicable trap geometry will make little difference in identifying the principal traps. However, more specific models may be necessary to resolve cases in which the concentration ranges of traps are close and even overlap.

RESULTS

PRECIPITATION-HARDENED ALLOYS

Inconel 718

Significant trapping is not observed before reduction of the surface film occurs; that is, values of k_a cannot be determined at low potentials, presumably because the entry flux at the oxide surface is so low that the amount of absorbed hydrogen does not vary appreciably with charging time. After the film was reduced at a sufficiently negative potential, the open-circuit potential tended to remain steady over the range of charging times for each subsequent overpotential, with virtually no tendency to shift back to the passive region between each charging time. The data at these potentials could be fitted to the interface control model, allowing trapping constants to be determined.

The values of k_a and J for two tests are given in Table 3. In both cases, k_a is independent of overpotential, as required for the diffusion/trapping model to be valid, because the traps are assumed to be unperturbed by electrochemical variables and remain unsaturated. The mean value of k_a is 0.031 ± 0.002 s^{-1}. The flux in general does not exhibit a significant change with overpotential. However, a small decrease occurs at -0.25 V, which could be related to possible hydride formation in the surface layer of the alloy or to hydrogen bubble formation on the surface at high cathodic potentials.

With the above value for k_a and the appropriate value of J used in Eq. (1), q_a was calculated for the full range of charging times (0.5-40 s) and compared with the corresponding experimental results. The two sets of data for the Inconel charged at $\eta = -0.15$ V in test 2 are shown in Figure 3. The close fit between them is typical for each overpotential and illustrates the independence of both k_a and J with respect to t_c.

The values of k_a and J were used to calculate the charge irreversibly trapped (q_T) and the ingress charge (q_{in}), and the charge ratios (q_T/q_{in} and q_{in}/q_c) were then obtained. The charge ratios are shown as a function of t_c in Figures 4 and 5. The fraction of hydrogen trapped (q_T/q_{in}) is found empirically to vary approximately linearly with $\sqrt{t_c}$, although the reason for this relatively simple dependence is not apparent from the more complex relationship between q_T and t_c. Some deviation from linearity occurs at long

13
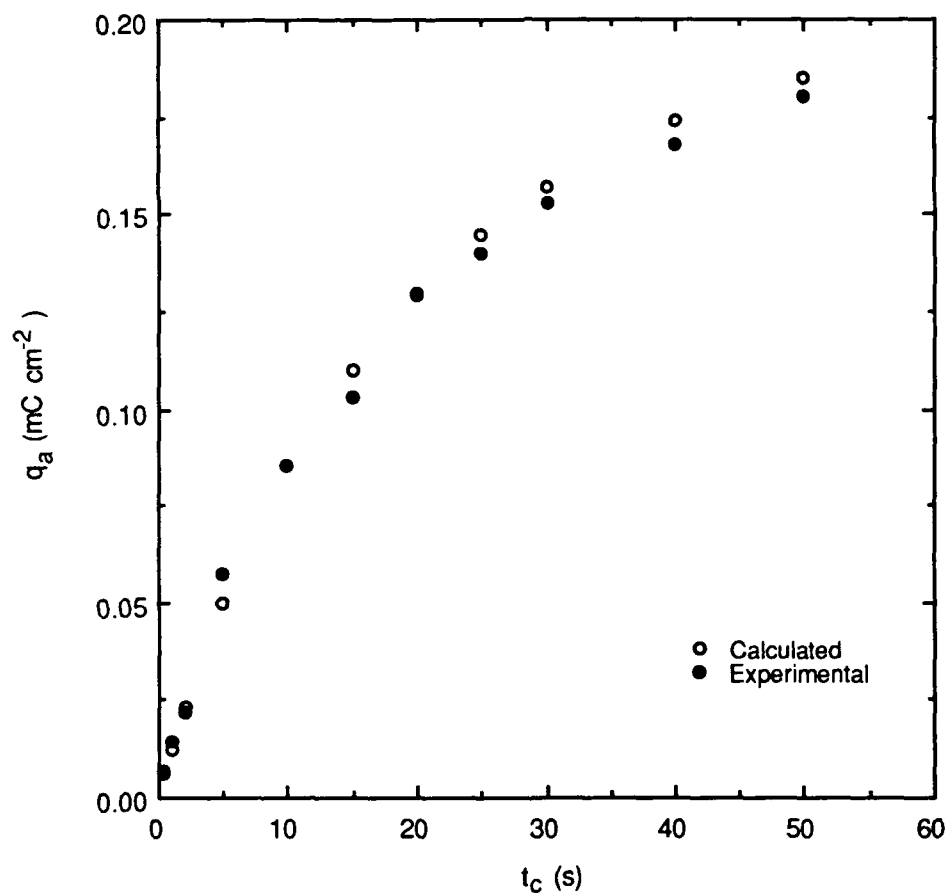
RA-1962-21

Figure 3. Comparison of experimental and calculated anodic charge
data for Inconel 718 in acetate buffer.

E_c = -0.671 V (SCE).

14
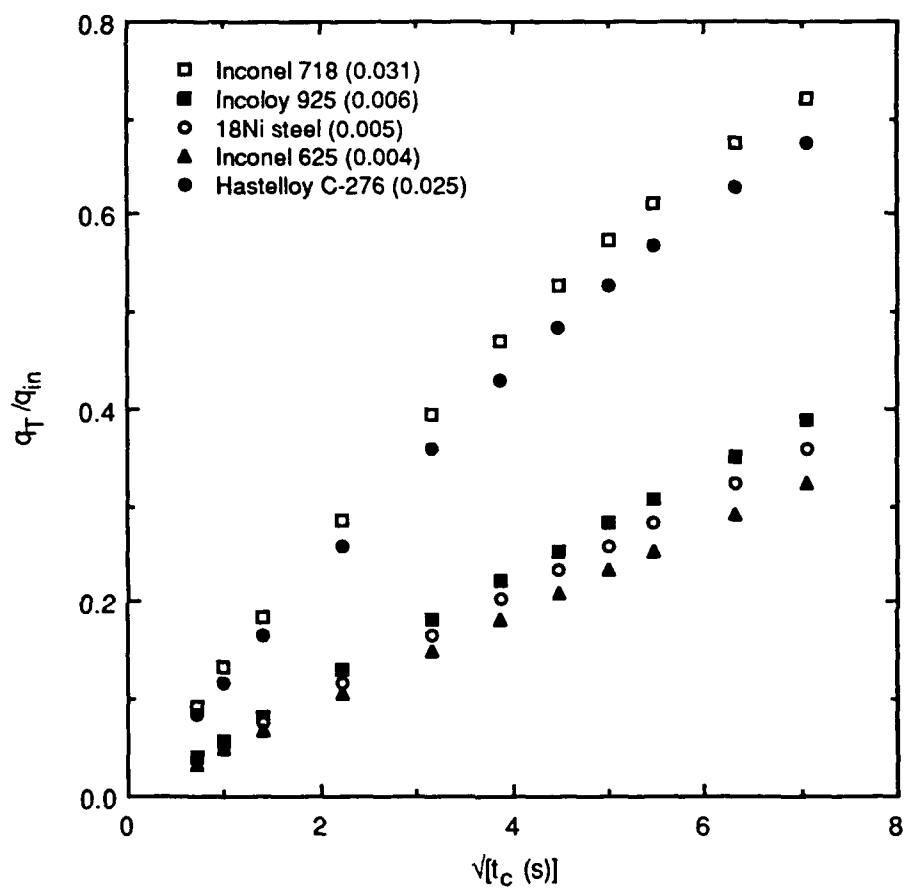
RA-1962-22

Figure 4. Dependence of q_T/q_{in} on charging time for Ni-containing alloys.

The apparent rate constants are given in parentheses for the particular alloy.
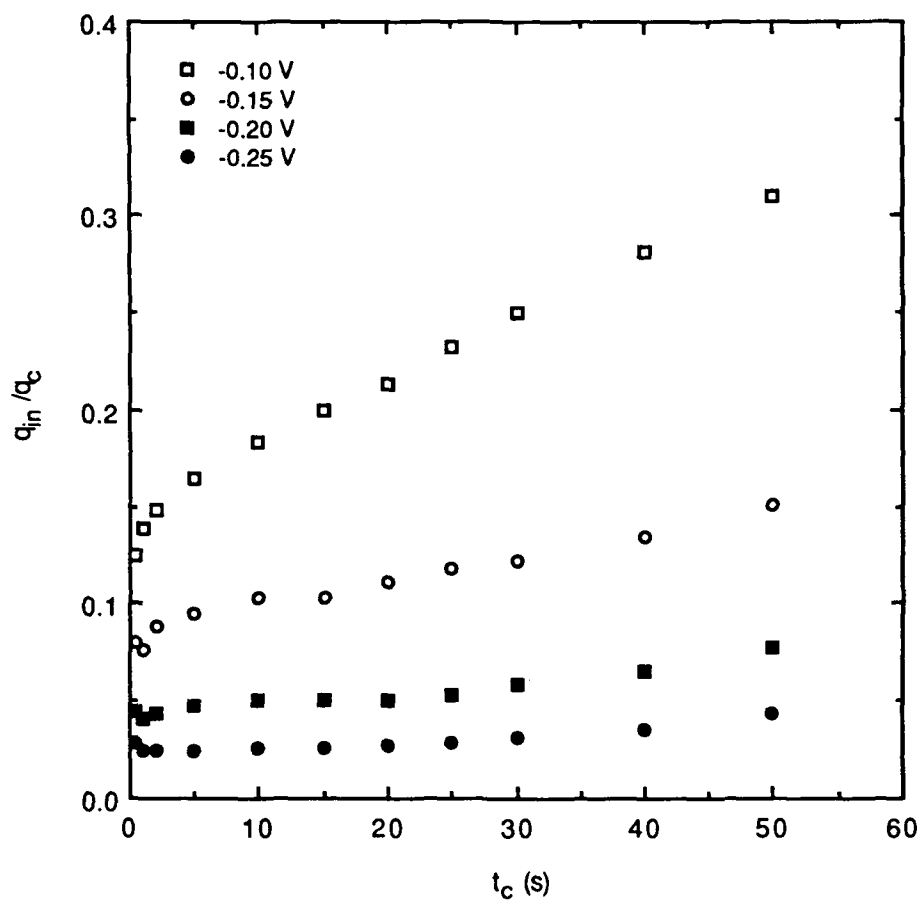
Figure 5. Dependence of q_{in}/q_c on charging time for Inconel 718 at various overpotentials.

RA-1962-23

charging times, which is to be expected in view of the different t_c dependence of q_T and q_{in}.

Table 3
VALUES OF k_a AND J FOR INCONEL 718

Test	η (V)	E_c (V/SCE)	k_a (s^{-1})	J (nmol cm^{-2} s^{-1})
2	-0.10	-0.616	0.031	0.13
	-0.15	-0.671	0.035	0.15
	-0.20	-0.731	0.028	0.12
	-0.25	-0.790	0.035	0.08
3	-0.15	-0.628	0.031	0.23
	-0.20	-0.713	0.030	0.22
	-0.25	-0.783	0.030	0.15

In contrast to q_T/q_{in}, the fraction of hydrogen entering the metal (q_{in}/q_c) is essentially constant with t_c for overpotentials from -0.15 V to -0.25 V. However, q_{in}/q_c increases almost linearly with t_c at -0.10 V and varies slightly even at -0.15 V. For a given charging time, q_{in}/q_c decreases with increasing overpotential, as shown more clearly in Figure 6. This decrease indicates that the rate of hydrogen desorption increases relative to the rate of hydrogen entry.

Incoloy 925

The values of k_a and J for four tests are given in Table 4. The low values of J imply that only a small amount of hydrogen entered the metal during t_c, and for this reason, obtaining precise values of q_a and therefore of k_a and J was difficult. Nevertheless, k_a does not appear to depend on overpotential and has a mean value of 0.006 ± 0.003 s^{-1}. Although the flux is small, it increases with overpotential. Values of q_a calculated using the derived values of k_a and J are compared with the corresponding experimental data ($\eta = -0.20$ V in test 10) in Figure 7, and again good agreement is observed over the range of charging times.

17
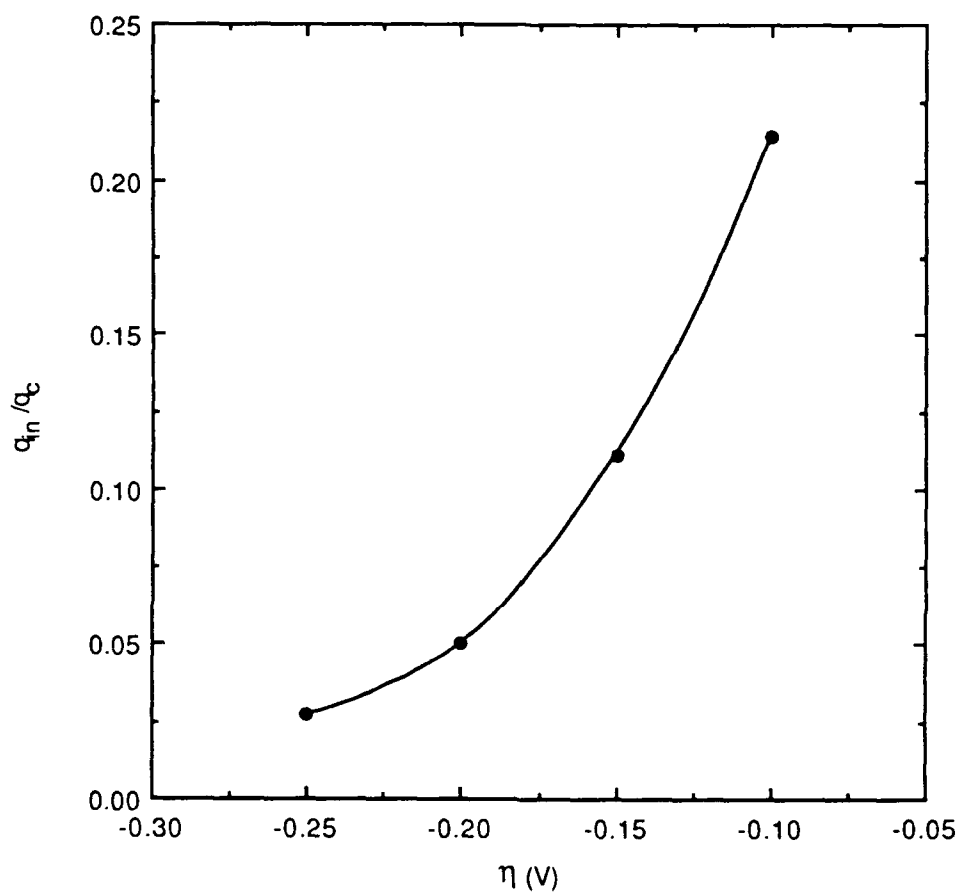
RA-1962-24

Figure 6. Dependence of q_{in}/q_c on overpotential for Inconel 718.
t_c = 20 s.

18
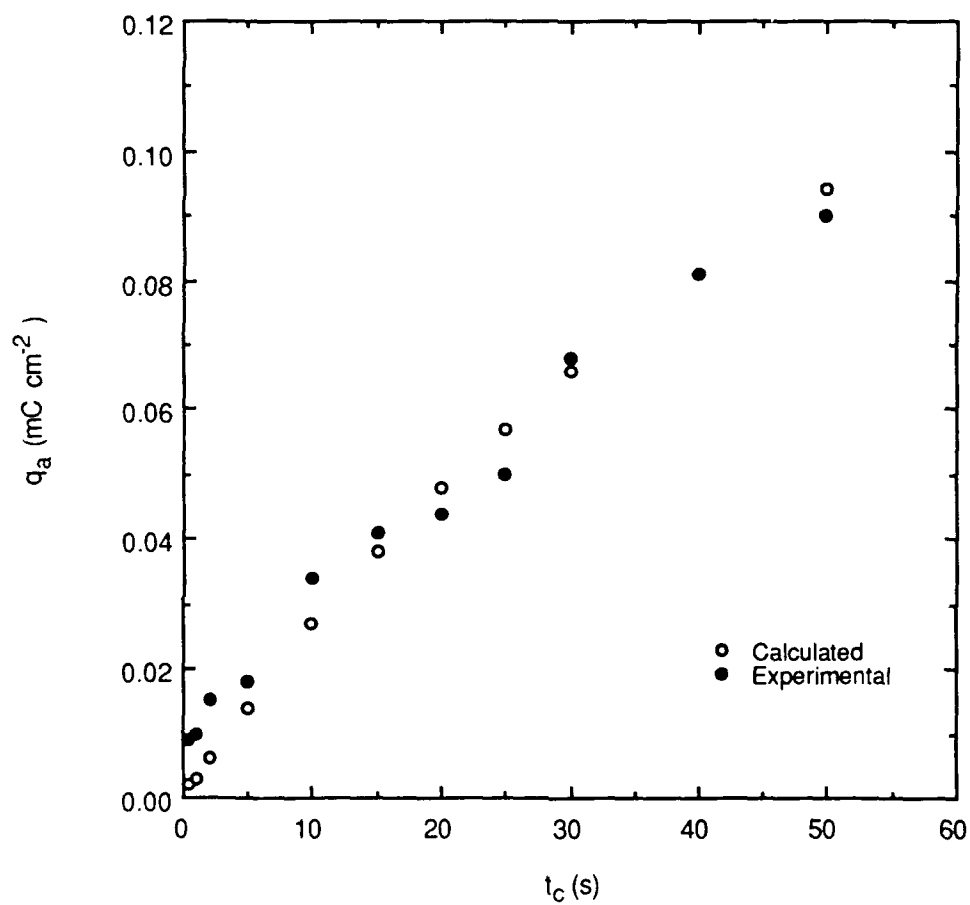
RA-1962-25

Figure 7. Comparison of experimental and calculated anodic charge
data for Incoloy 925 in acetate buffer.

$E_c = -0.369$ V (SCE).

Data for q_T/q_{in} are shown in Figure 4. The charging current and therefore the cathodic charge (q_c) were low for the Incoloy, so it was not possible to determine reliable values for q_{in}/q_c. Unlike Inconel 718, the Incoloy shows a linear dependence of q_T/q_{in} on $\sqrt{t_c}$ over the full range of charging times studied, evidently as a result of its lower trapping constant.

Table 4
VALUES OF k_a AND J FOR INCOLOY 925

Test	η (V)	E_c (V/SCE)	k_a (s^{-1})	J (nmol cm^{-2} s^{-1})
9	-0.25	-0.382	0.001	0.02
	-0.30	-0.458	0.009	0.05
10	-0.20	-0.369	0.008	0.04
	-0.25	-0.414	0.011	0.05
	-0.30	-0.476	0.003	0.08
11	-0.25	-0.367	0.003	0.03
	-0.30	-0.427	0.006	0.06
12	-0.20	-0.383	0.005	0.02

18Ni Maraging Steel

The values of k_a and J for four tests are given in Table 5. The tests were performed in two pairs, with the two tests in a pair performed 1 hr apart and the two pairs separated by ~18 hr. The values of k_a for three of the tests (27, 28, and 30) are essentially independent of potential. Also, the flux in these tests shows a small but systematic increase with overpotential. However, the trapping constants for test 27 are noticeably higher than those for test 28. Similarly, the k_a values for test 29 up to -0.2 V are higher than the corresponding values in test 30 but then decrease to values similar to those in tests 28 and 30.

The decrease in k_a suggests a filling of some traps, presumably to saturation level because k_a eventually becomes constant. In contrast, the change in k_a over 18 hr indicates that the traps are emptied over this period. This explanation implies that hydrogen

20

diffusion either through the lattice or along grain boundaries in maraging steel is rapid enough to penetrate beyond the layer of metal removed during polishing before each test.

Table 5
VALUES OF k_a AND J FOR 18NI MARAGING STEEL

Test	η (V)	E_c (V/SCE)	k_a (s^{-1})	J ($nmol\ cm^{-2}\ s^{-1}$)	Mean k_a
27	-0.10	-0.549	0.025	0.13	
	-0.15	-0.601	0.010	0.12	
	-0.20	-0.677	0.014	0.13	
	-0.25	-0.747	0.011	0.13	0.015 ± 0.003
	-0.30	-0.806	0.014	0.15	
	-0.35	-0.866	0.015	0.17	
	-0.40	-0.925	0.016	0.19	
28	-0.10	-0.600	0.003	0.04	
	-0.15	-0.655	0.007	0.06	
	-0.20	-0.710	0.003	0.07	
	-0.25	-0.768	0.004	0.08	0.006 ± 0.002
	-0.30	-0.826	0.006	0.09	
	-0.35	-0.881	0.007	0.11	
	-0.40	-0.940	0.010	0.14	
29	-0.10	-0.556	0.021	0.11	
	-0.15	-0.620	0.014	0.10	
	-0.20	-0.684	0.021	0.13	
	-0.25	-0.747	0.015	0.10	*
	-0.30	-0.806	0.007	0.09	
	-0.35	-0.863	0.004	0.10	
	-0.40	-0.919	0.008	0.12	
30	-0.10	-0.600	0.008	0.04	
	-0.15	-0.659	0.001	0.04	
	-0.20	-0.714	0.004	0.06	
	-0.25	-0.771	0.002	0.07	0.005 ± 0.002
	-0.30	-0.827	0.004	0.08	
	-0.35	-0.876	0.008	0.10	
	-0.40	-0.932	0.005	0.11	

* Mean not calculated because k_a changed at high overpotentials.

If residual hydrogen is assumed to be present, the change in trapping behavior can be explained by the effects of different types of traps. The apparent trapping constants for

tests 27 and 29 probably reflect a combination of truly irreversible and quasi-irreversible traps (traps that are irreversible over minutes up to at least 1 hr but not for longer times spanning hours), whereas those for tests 28 and 30 are assumed to correspond to irreversible trapping only. In irreversible trapping, the rate constant for release is assumed to be zero, whereas in the quasi-irreversible case, the release constant is not zero but is too small to achieve local equilibrium between the lattice and the trapped hydrogen.

The densities of the irreversible and quasi-irreversible traps are assumed to be additive, so that in accordance with Eq. (4), k_a can be separated into two components:

$$k_a = k_a' + k_a''$$ (5)

where k_a' and k_a'' correspond to the irreversible and quasi-irreversible traps, respectively. The total trapping constant was determined as the mean of the results from test 27, giving $k_a = 0.015 \pm 0.003$ s^{-1}. The results for test 29 apparently reflect a transition from combined trapping to only irreversible trapping. The irreversible trapping constant was obtained as the mean of the results from tests 28 and 30, so that $k_a' = 0.005 \pm 0.002$ s^{-1} and therefore $k_a'' = 0.010 \pm 0.005$ s^{-1}.

Values of q_a calculated using k_a and J are compared with the corresponding experimental results ($\eta = -0.35$ V in test 28) in Figure 8, in which it is evident that the data are in close agreement over the full range of charging times.

Data for the charge ratios as a function of t_c are shown in Figures 4 and 9. The ratio of q_T to q_{in} for the maraging steel is linearly dependent on $\sqrt{t_c}$ over the range of interest. As with Inconel 718, q_{in}/q_c is virtually independent of t_c at higher overpotentials, but shows a slight dependence as the overpotential decreases. Also, q_{in}/q_c decreases with increasing overpotential (Figure 10), again probably reflecting the relative increase in the rate of hydrogen desorption over hydrogen entry.
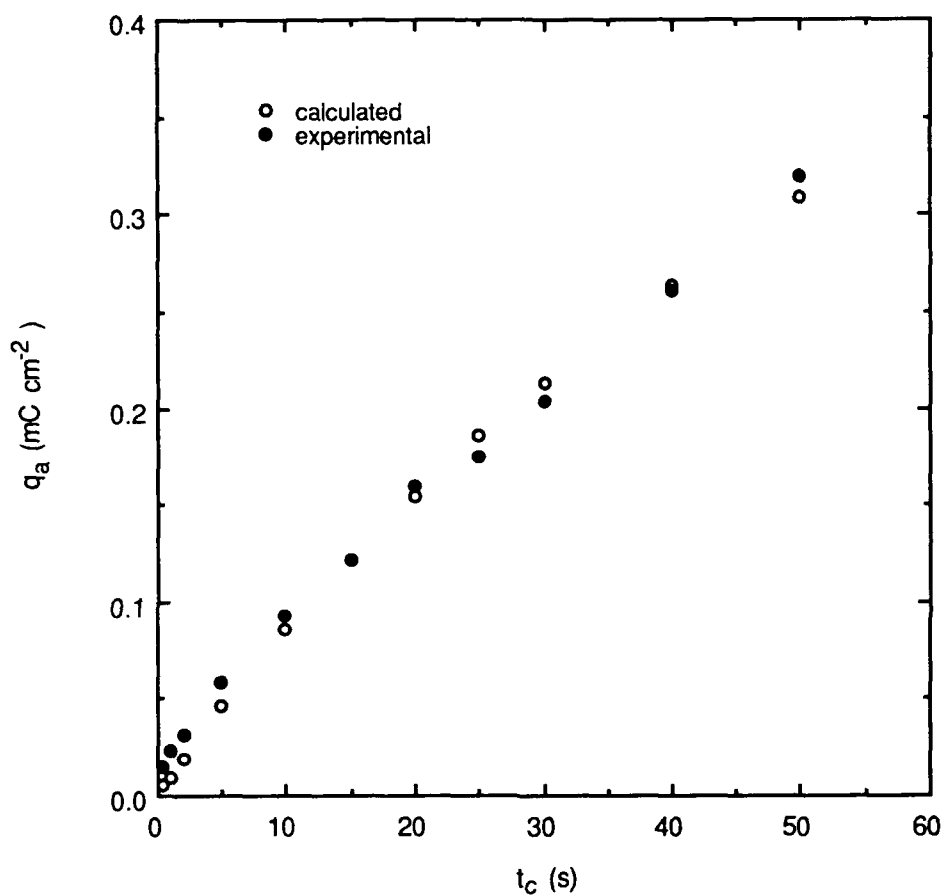
RAM-1962-26

Figure 8. Comparison of experimental and calculated anodic charge data for 18Ni maraging steel in acetate buffer.

$E_c = -0.881$ V (SCE)

23
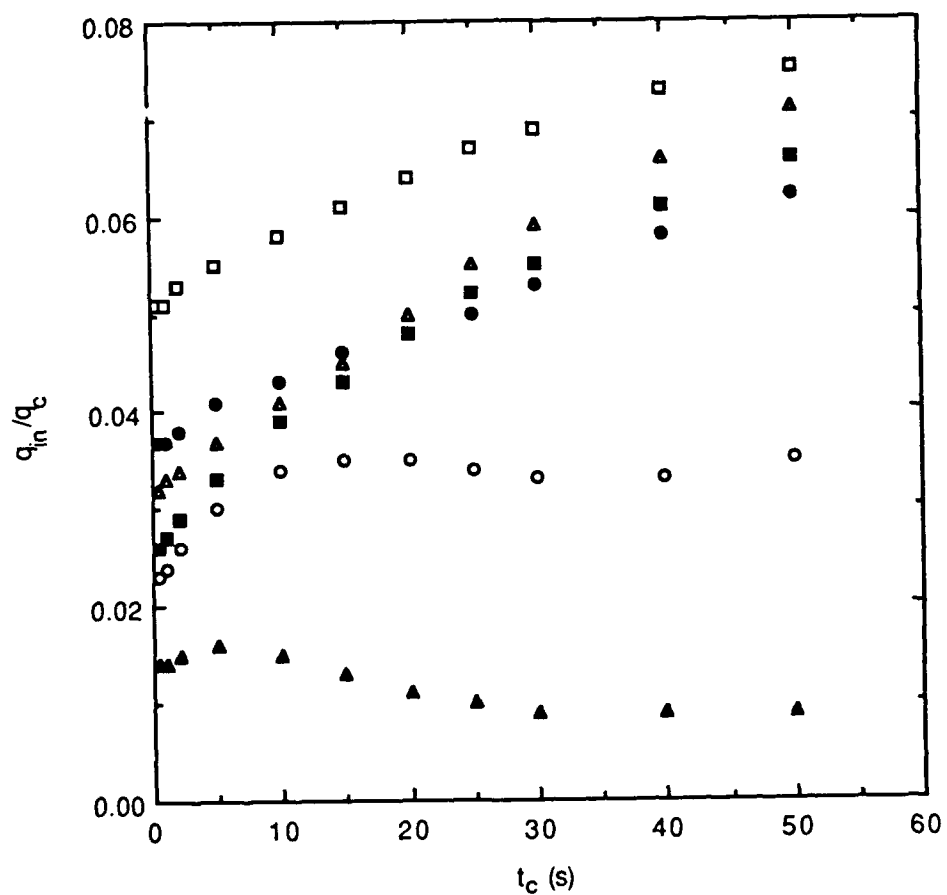
RAM-1962-27

Figure 9. Dependence of q_{in}/q_c on charging time for 18Ni maraging steel at various overpotentials.

□ -0.15 V; ● -0.20 V; ▲ -0.25 V; ■ -0.30 V;
○ -0.35 V; ▲ -0.40 V.

RA-1962-28
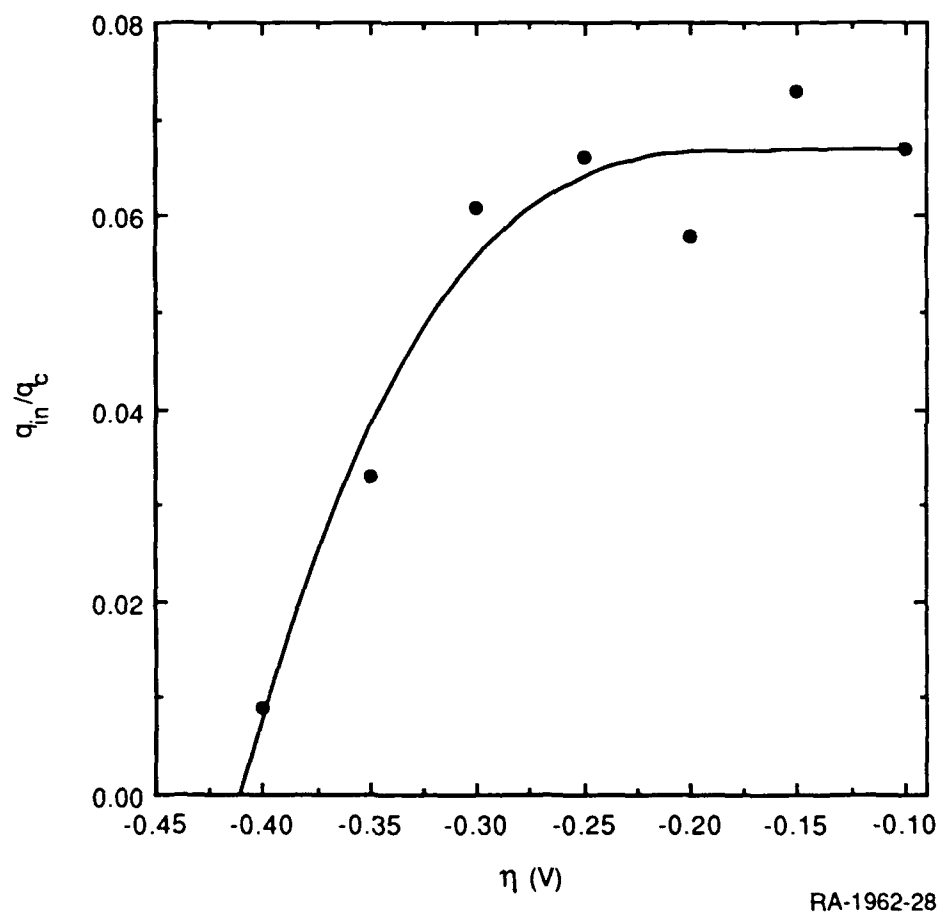
Figure 10. Dependence of q_{in}/q_c on overpotential for 18Ni maraging steel.

$t_c = 40$ s.

WORK-HARDENED ALLOYS

Inconel 625

Values of k_a and J for four tests are given in Table 6. The ingress flux for this alloy, like that of Incoloy 925, was small, so that it was difficult to determine precise values for k_a and J. However, k_a varied over a relatively small range from 0.001 to 0.008 s^{-1} with a mean value of 0.004 ± 0.002 s^{-1}. Values of q_a calculated using the derived values of k_a and J are compared with the corresponding experimental data ($\eta = -0.10$ V in test 37) in Figure 11, and again good agreement is observed over the range of charging times.

Table 6
VALUES OF k_a AND J FOR INCONEL 625

Test	η (V)	E_c (V/SCE)	k_a (s^{-1})	J (nmol cm^{-2} s^{-1})
35	-0.20	-0.355	0.006	0.01
36	-0.10	-0.391	0.001	0.01
37	-0.10	-0.378	0.004	0.01
	-0.15	-0.433	0.002	0.02
38	-0.05	-0.527	0.008	0.03

Data for q_T/q_{in} are shown in Figure 4. As with Incoloy 925, the cathodic charge was low for Inconel 625, so the values of q_{in}/q_c were not reliable for this alloy either. Like the Incoloy and maraging steel, Inconel 625 shows a linear dependence of q_T/q_{in} on $\sqrt{t_c}$, again apparently because of the relatively low influence of trapping on hydrogen ingress.

Hastelloy C-276

Significant trapping in this alloy, as with Inconel 718, is not observed before the surface film is reduced. After film reduction, the open-circuit potential, like that for the Inconel, remained steady over the range of charging times for each subsequent
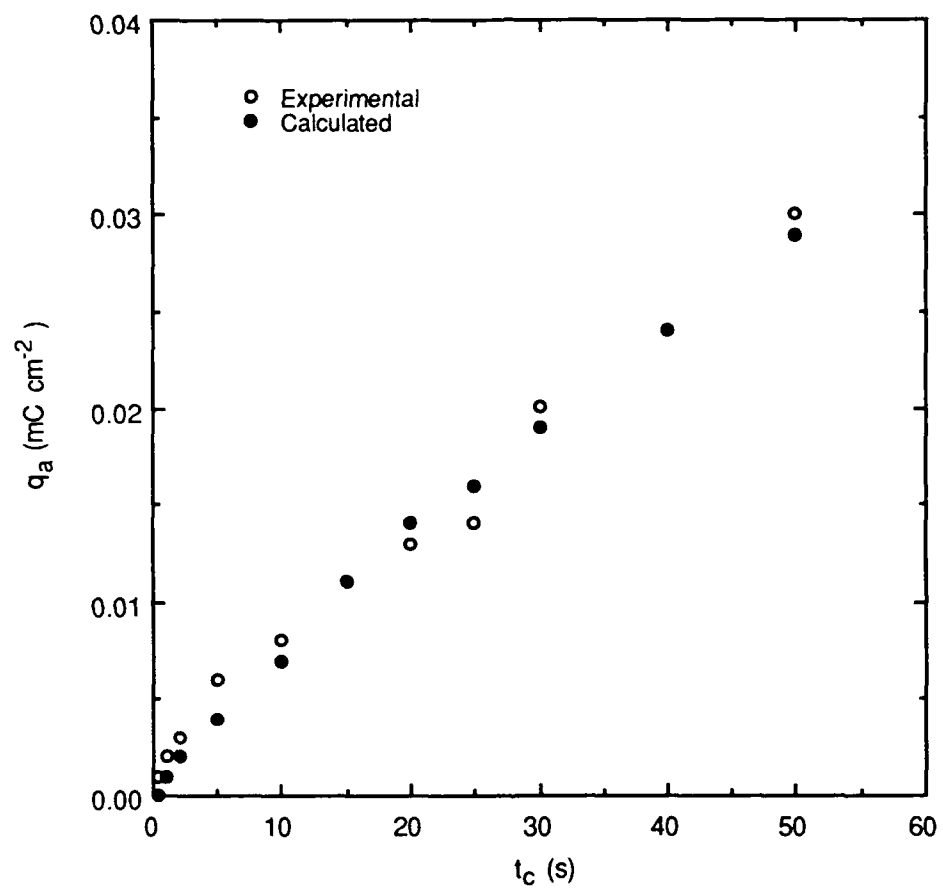
RAM-1962-36

Figure 11. Comparison of experimental and calculated anodic charge
data for Inconel 625 in acetate buffer.

E_c = -0.378 V (SCE).

27

overpotential. Data were fitted to the interface control model, and values determined for k_a and J are given in Table 7.

Table 7
VALUES OF k_a AND J FOR HASTELLOY C-276

Test	η (V)	E_c (V/SCE)	k_a (s^{-1})	J (nmol cm^{-2} s^{-1})
31	-0.25	-0.748	0.061	0.27
32	-0.10	-0.593	0.025	0.06
	-0.15	-0.658	0.033	0.08
	-0.20	-0.725	0.023	0.04
	-0.30	-0.851	0.020	0 01
	-0.35	-0.895	0.026	0.02
33	-0.25	-0.754	0.041	0.22
	-0.30	-0.813	0.049	0.12
34	-0.20	-0.702	0.036	0.17
	-0.25	-0.762	0.041	0.12
	-0.30	-0.848	0.037	0.06

Two pairs of tests (31, 32 and 33, 34) for the Hastelloy were performed about 18 hr apart, with 1 and 1.5 hr between the tests in the first and second pair, respectively. Film reduction was evident from a marked negative shift in E_{oc} in tests 31, 33, and 34 and occurred in the region of $E_c = -0.52$ V (η = -0.20 to -0.25 V). In test 32, E_{oc} was negative of the potential for film reduction even at low overpotentials, indicating that the oxide film was absent at any stage in this test. Data for the charge at high overpotentials in each test were limited by the onset of significant bubble formation on the electrode surface, usually at η = -0.35 V. Nevertheless, the values of k_a for overpotentials immediately after film reduction are typically somewhat higher than those in test 32; such changes in k_a were not observed for Inconel 718, suggesting that the type of trap detected immediately after film reduction for the Hastelloy is different from that for the Inconel.

The trapped hydrogen corresponding to the high k_a values apparently remains in the test specimen between consecutive tests performed 1 hr apart despite repolishing of the electrode. The eventual decrease in k_a between tests 31 and 32 suggests that one type of

trap is filled to saturation but, over a sufficient time ($\geq$1.5 hr), the hydrogen in these traps is released, as reflected by the change in results between tests 33 and 34. The decrease in J observed in tests 33 and 34 suggests that the trapping associated with the high k_a values involves hydride formation in the surface layer of the alloy (discussed later).

The overall trapping behavior can be interpreted in terms similar to those for the maraging steel. Thus, the high trapping constants for tests 31, 33, and 34 are thought to represent a combination of irreversible and quasi-irreversible traps, so k_a can be separated into two components, k_a' and k_a'', respectively. The total trapping constant was determined as the mean of the results from tests 31, 33, and 34, giving $k_a = 0.044 \pm 0.007$ s^{-1}. The apparent rate constant for irreversible trapping was obtained as the mean of the results from test 32, so $k_a' = 0.025 \pm 0.003$ s^{-1}, and therefore $k_a'' = 0.019 \pm 0.010$ s^{-1}. A comparison of calculated and experimental data for q_a ($\eta = -0.20$ V in test 32) in Figure 12 again indicates that the derived values of k_a and J are independent of charging time over the range studied.

Data for the charge ratios as a function of t_c are shown in Figures 4 and 13. As with Inconel 718, q_T/q_{in} for the Hastelloy shows some deviation from a linear dependence on $\sqrt{t_c}$ at long charging times. Also, q_{in}/q_c is largely independent of t_c at higher overpotentials and decreases with increasing overpotential (Figure 14), no doubt for the same reason of enhanced hydrogen desorption relative to hydrogen entry.

TITANIUM

Pure Titanium

The anodic charge (q_a) was invariant with t_c, which is not predicted by the diffusion/trapping model for either diffusion or interface control. Therefore, k_a could not be determined at any potential over the wide range studied (-0.05 V to -0.8 V). The open-circuit potential, and therefore the charging potential, generally showed a positive shift over the range of charging times for each overpotential. This shift might compensate for the increase in t_c. However, in several cases, E_c changed by $\leq$5 mV and q_a was essentially constant. Therefore, any effect resulting from the shift in E_c appears to be minor. Instead, the invariance in q_a indicates that negligible hydrogen enters the metal, so q_{in} is approximately zero, and therefore q_a corresponds solely to oxidation of the adsorbed layer of hydrogen; that is, it should comprise only q_{ads}. The dependence of log q_a on η (Figure 15) is linear over a wide potential range, as expected if $q_a \sim q_{ads}$. The lack of

29
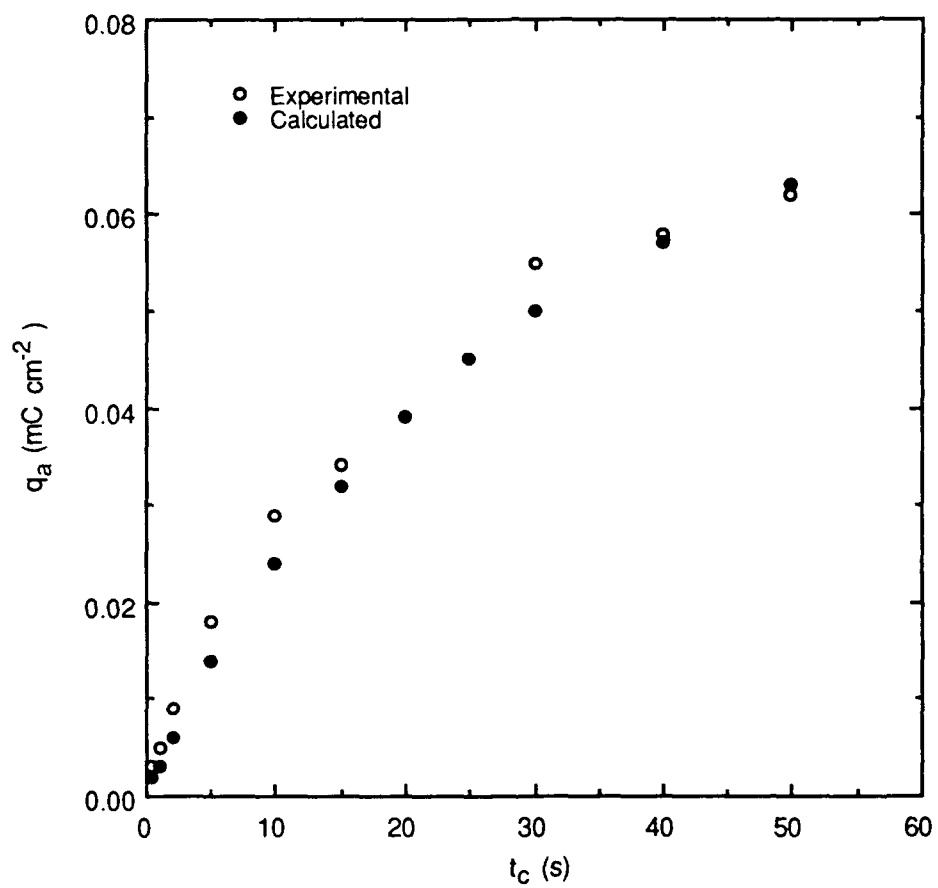
Figure 12. Comparison of experimental and calculated anodic charge data for Hastelloy C-276 in acetate buffer.

$E_c = -0.725$ V (SCE).
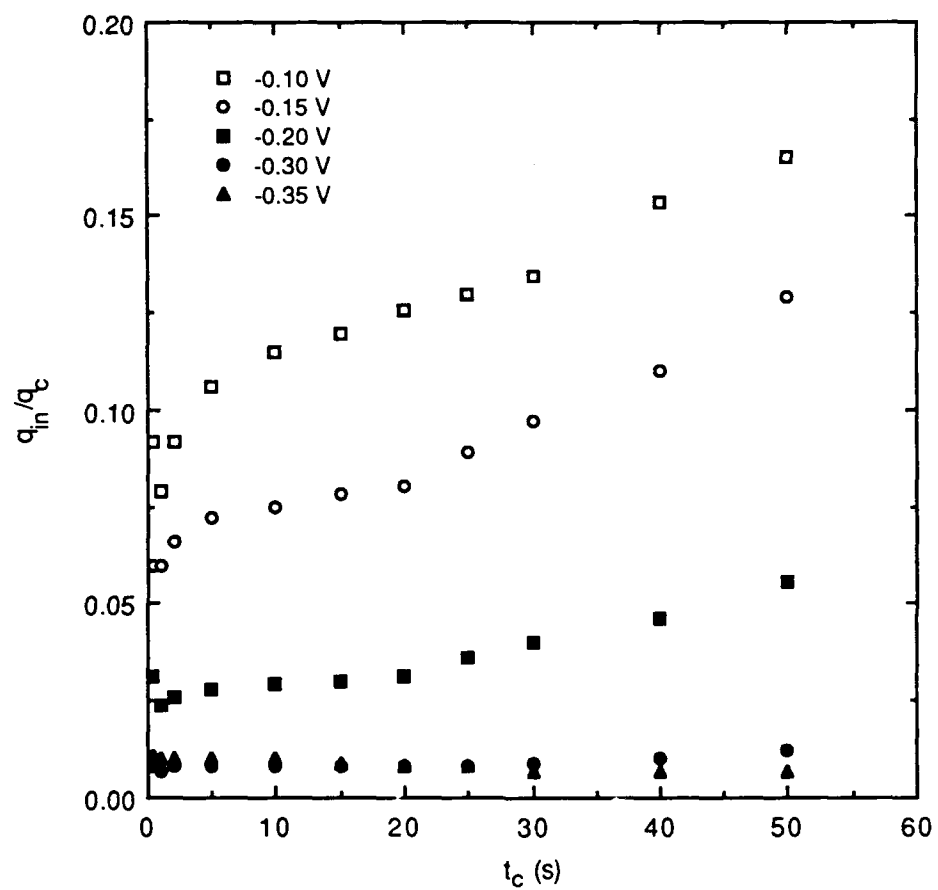
RAM-1962-38

Figure 13. Dependence of q_{in}/q_c on charging time for Hastelloy C-276 at various overpotentials.

31
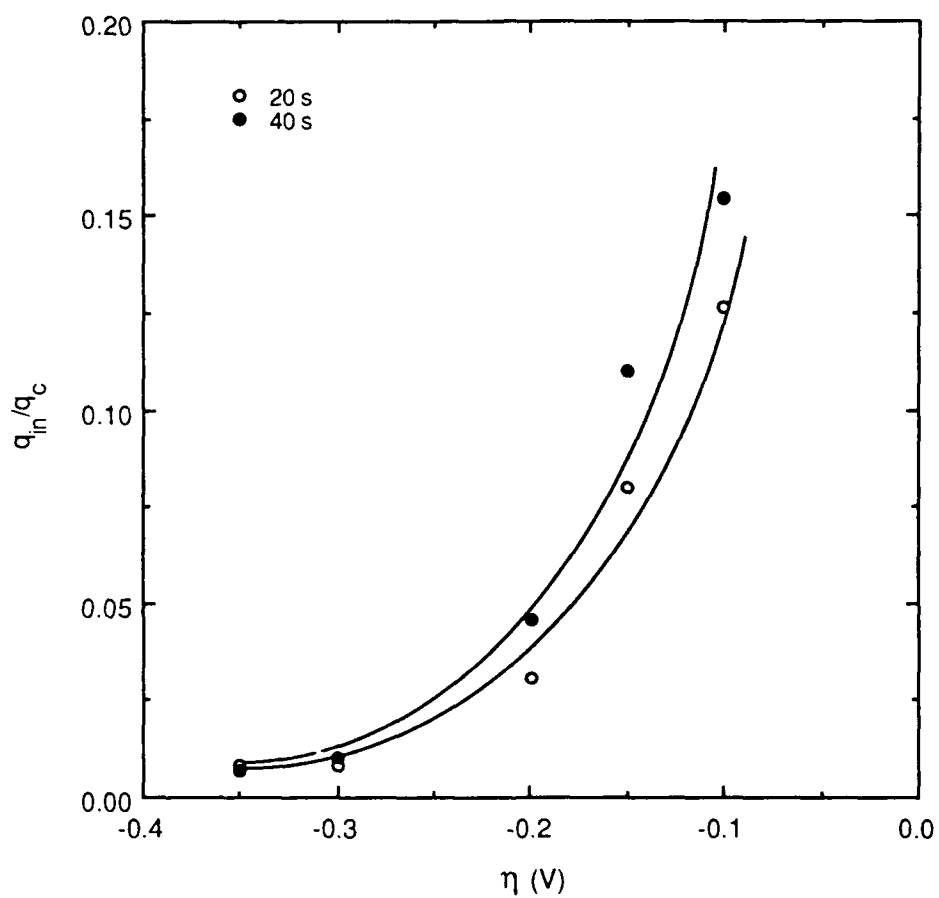
RAM-1962-39

Figure 14. Dependence of q_{in}/q_c on overpotential for Hastelloy C-276 at charging times of 20 and 40 s.

Figure 15. Dependence of anodic charge on overpotential for pure titanium in acetate buffer.

RA-1962-29

33

dependence at high overpotentials probably corresponds to full coverage of the adsorbed hydrogen layer.

Titanium Grade 2

Titanium grade 2, in contrast to the pure form, shows a marked dependence of q_a on t_c, so trapping constants can be evaluated in this case. Four tests were performed, and the values of k_a and J given in Table 8 for two of the tests are typical of the overall results. The flux increases with overpotential as a result of the dependence of J on the surface coverage of H_{ads}. The variation in log J with η shown in Figure 16 is linear, as is required with the assumption that the surface coverage responded rapidly to changes in potential.

In both tests, k_a is independent of overpotential but exhibits two valu.ᵔ ᵤ̣pending on the potential range. At charging potentials up to approximately -0.93 V, k_a is 0.028 ± 0.002 s^{-1}, whereas the mean value at higher potentials is 0.040 s^{-1}. The two other tests gave trapping constants of 0.036 s^{-1} and 0.042 s^{-1} at high potentials, so that the mean value of k_a at high potentials in the four tests was 0.040 ± 0.004 s^{-1}. Values of q_a calculated using k_a and J are compared with the corresponding experimental data ($\eta = -0.70$ V in test 23) in Figure 17, and again the data agree well over the charging time range.

The increase in trapping constant at high overpotentials can be ascribed to another type of irreversible trap participating concurrently with those detected at low overpotentials. The densities of the two traps are assumed to be additive, and therefore k_a at high overpotentials can be represented by

$$k_a = k_{a1} + k_{a2} \tag{6}$$

where k_{a1} corresponds to the irreversible traps detected at low η and k_{a2} is associated with the other type of trap. The total trapping constant (k_a) was taken as the mean (0.040 s^{-1}) of the high η results, and $k_{a1} = 0.028 \pm 0.002$ s^{-1}, so that $k_{a2} = 0.012 \pm 0.006$ s^{-1}.

Data for the charge ratios as a function of t_c at low overpotentials are shown in Figures 18 and 19. As with Inconel 718 and the Hastelloy, q_T/q_{in} for titanium grade 2 shows some deviation from the empirical $\sqrt{t_c}$ dependence, which is likewise related to its relatively high trapping constant. The ratio of q_{in} to q_c increases with t_c. However, in contrast to that for the nickel-containing alloys, this increase in q_{in}/q_c becomes greater at higher overpotentials (Figure 20), indicating that hydrogen entry becomes more efficient.

34
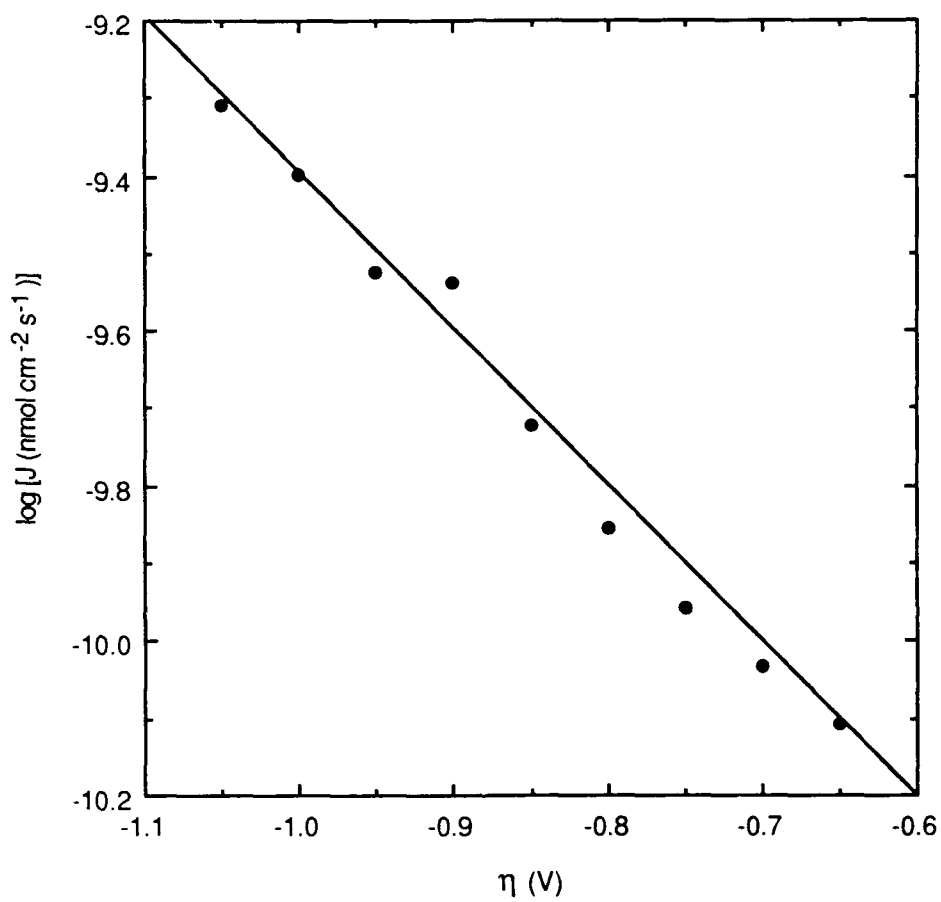
RA-1962-30

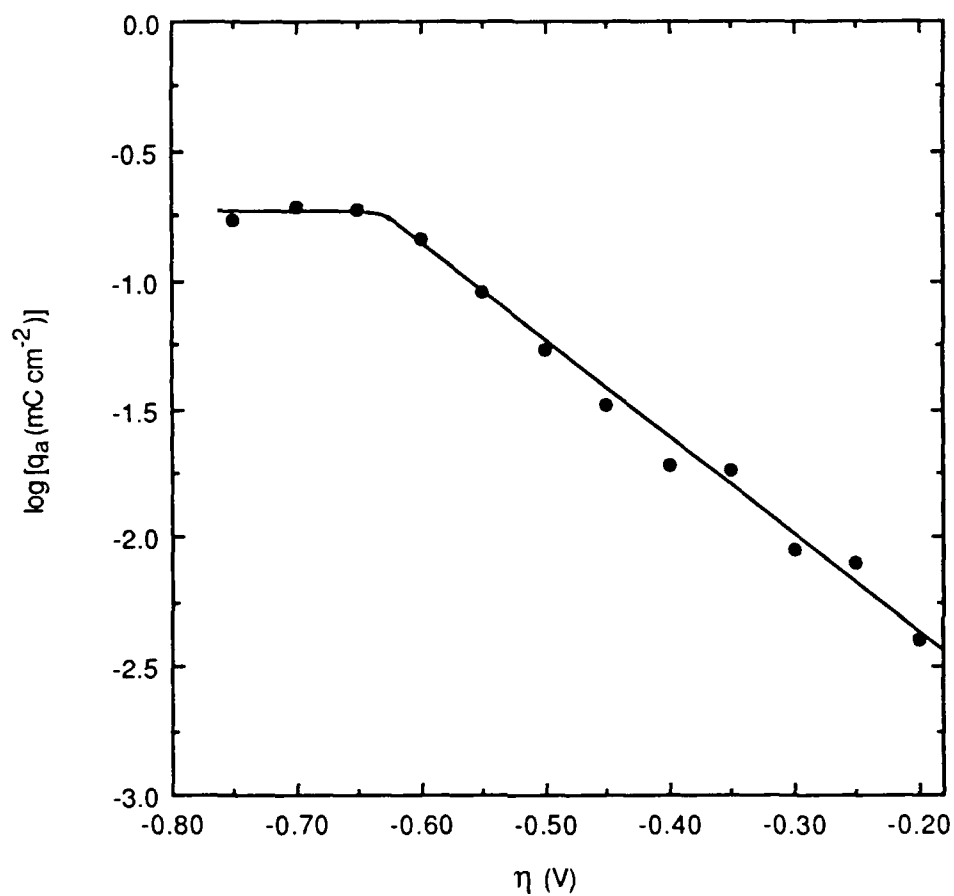Figure 16. Dependence of flux on overpotential for titanium grade 2.
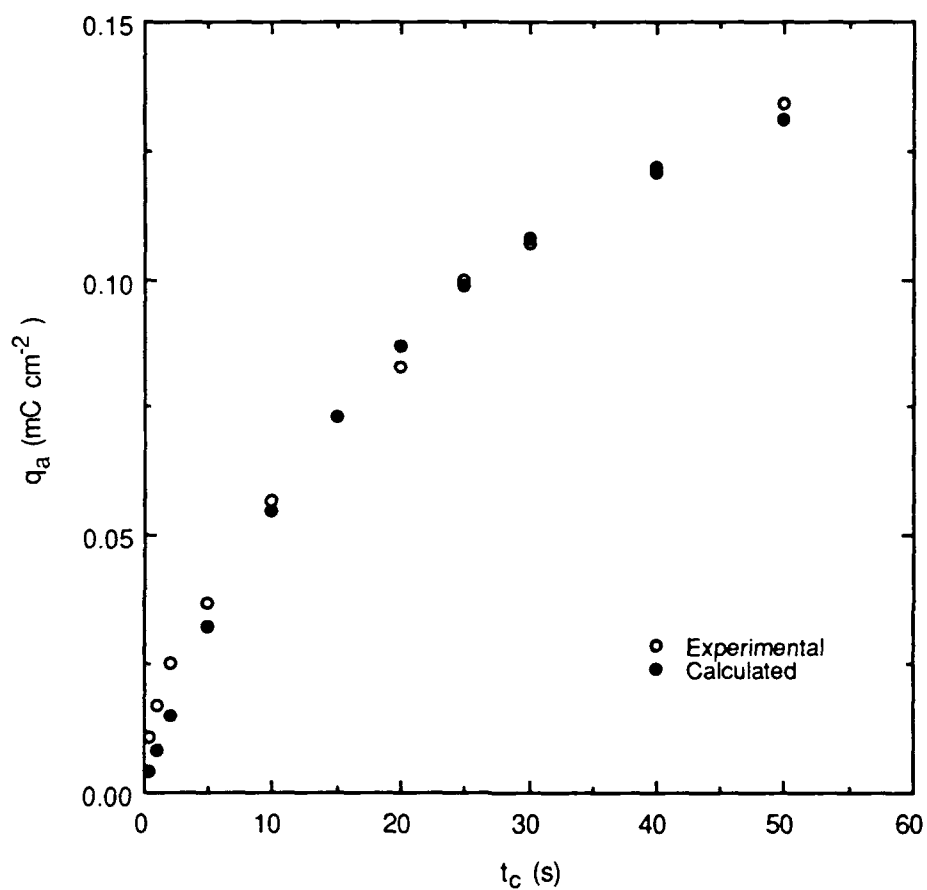
RA-1962-31

Figure 17. Comparison of experimental and calculated anodic charge
data for titanium grade 2 in acetate buffer.

$E_c = -0.741$ V (SCE).

36
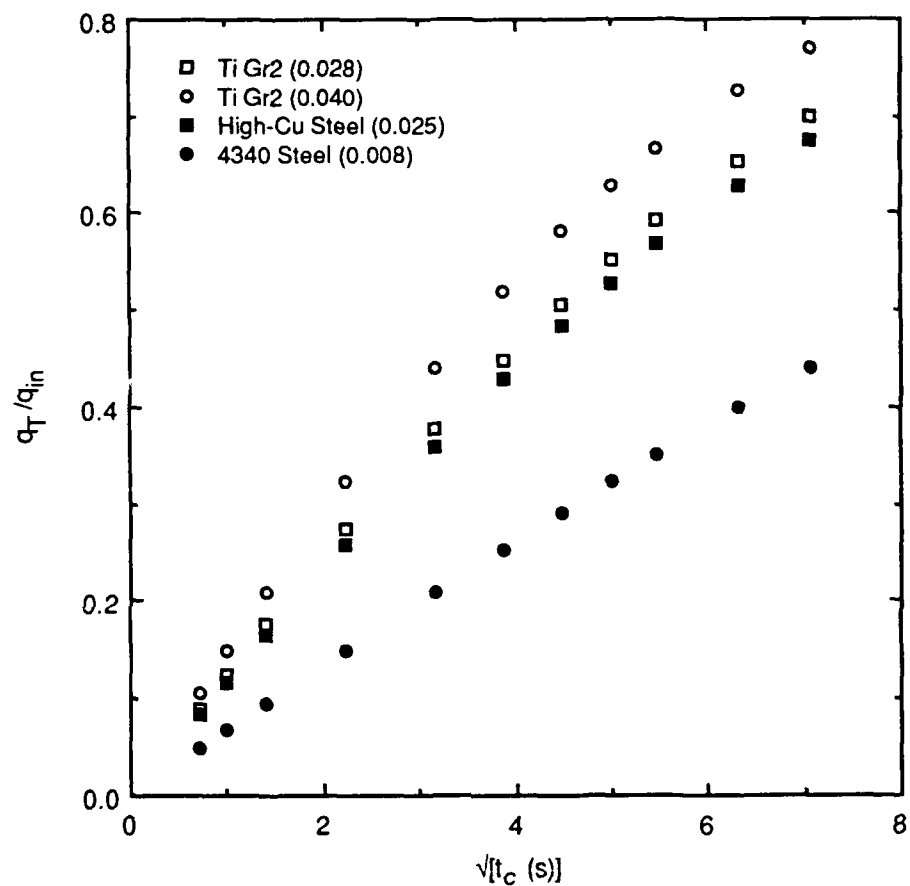
Figure 18. Dependence of q_T/q_{in} on charging time for titanium grade 2 and 4340 steel (HRC 53 and high Cu).

The apparent rate constants are given in parentheses for the particular alloy.

37
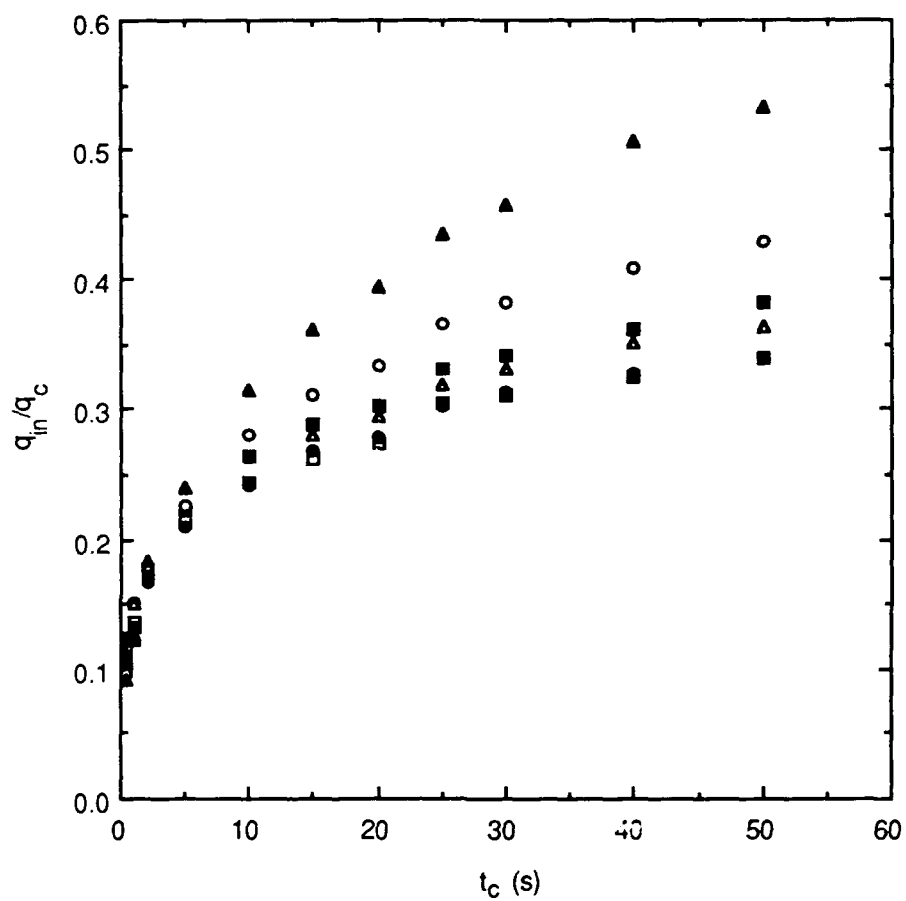
RA-1962-32

Figure 19.   Dependence of q_{in}/q_c on charging time for titanium
grade 2 at low overpotentials.

□   -0.60 V ; ●   -0.65 V ; ▲   -0.70 V ; ■   -0.75 V ;
○   -0.80 V ; ▲   -0.85 V.
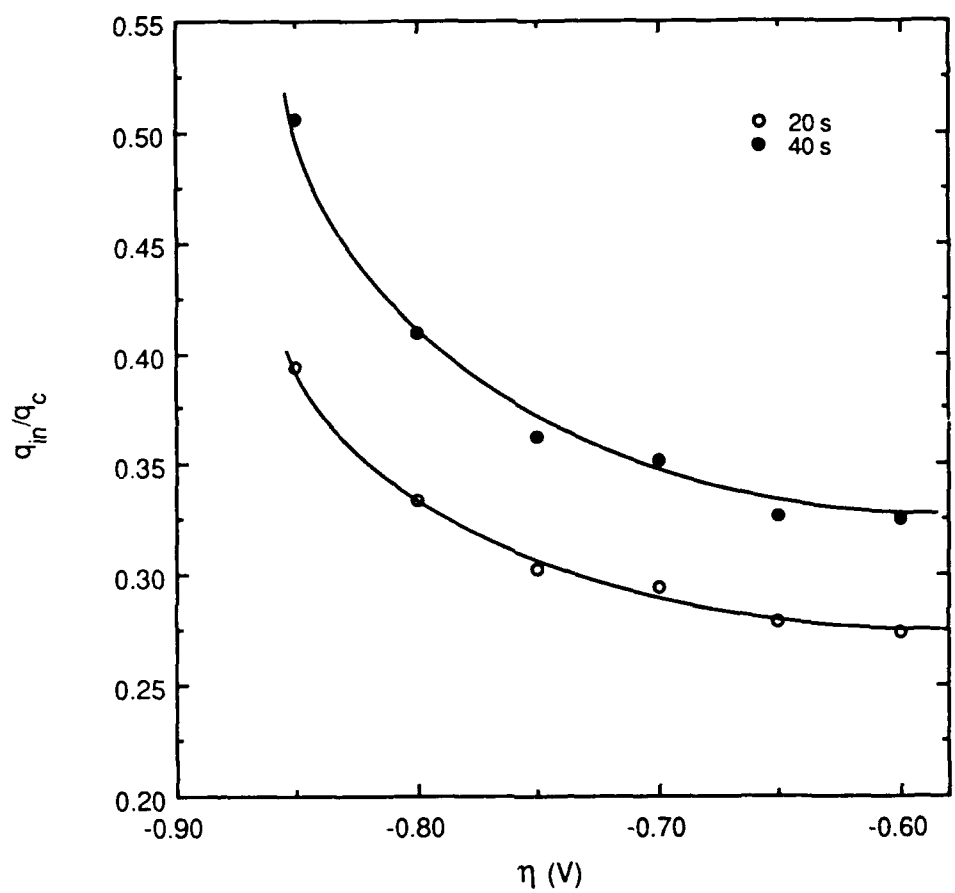
Figure 20. Dependence of q_{in}/q_c on overpotential for titanium grade 2 at low overpotentials and charging times of 20 and 40 s.

Table 8
VALUES OF k_a AND J FOR TITANIUM GRADE 2

Test	η (V)	E_c (V/SCE)	k_a (s^{-1})	J ($nmol\ cm^{-2} s^{-1}$)	Mean k_a
21	-0.55	-0.614	0.029	0.07	
	-0.60	-0.652	0.034	0.08	
	-0.65	-0.708	0.025	0.08	
	-0.70	-0.751	0.024	0.09	0.028 ± 0.002
	-0.75	-0.806	0.028	0.13	
	-0.80	-0.868	0.029	0.17	
	-0.85	-0.930	0.029	0.22	
	-0.90	-1.040	0.044	0.39	
	-0.95	-1.062	0.044	0.44	
	-1.00	-1.137	0.049	0.56	0.044 ± 0.002
	-1.05	-1.203	0.042	0.59	
	-1.10	-1.283	0.044	0.69	
	-1.15	-1.370	0.041	0.73	
23	-0.60	-0.655	0.031	0.07	
	-0.65	-0.692	0.028	0.08	
	-0.70	-0.741	0.029	0.09	0.028 ± 0.001
	-0.75	-0.796	0.027	0.11	
	-0.80	-0.857	0.027	0.14	
	-0.85	-0.921	0.028	0.19	
	-0.90	-0.987	0.034	0.29	
	-0.95	-1.024	0.033	0.30	
	-1.00	-1.111	0.039	0.40	0.036 ± 0.003
	-1.05	-1.182	0.041	0.49	
	-1.10	-1.258	0.035	0.49	
	-1.15	-1.310	0.034	0.51	

Therefore, hydrogen atom recombination during charging on Ti grade 2 must occur electrochemically because chemical recombination should become more efficient than entry at high overpotentials owing to the different dependence of their rates on surface coverage. A similar result was obtained in studies[12] of titanium in sulfuric acid solutions between pH 0.25 and 2.25; under these conditions, hydrogen evolution is believed to occur on an oxide film at potentials more positive than approximately -1.0 V and to involve electrochemical desorption as the rate-determining step.

The data for q_T/q_{in} at high overpotentials shows nonlinear behavior similar to that for this ratio at low overpotentials (Figure 18). Also, q_{in}/q_c in general increases with t_c, as shown in Figure 21, but varies with η in a manner opposite that found for low overpotentials; that is, q_{in}/q_c is high at the low end of the overpotential range and decreases as η increases (Figure 22). This reduction in the efficiency of hydrogen entry can be explained by the formation of a hydride, as will be discussed later.

COPPER-ENRICHED HIGH-STRENGTH STEEL

Values for the flux and trapping constants of both the high-Cu and heat-treated (HRC 53) 4340 steel are given in Table 9. The trapping constant for the high-Cu steel is independent of potential, as found earlier for the HRC 53 steel, and has a mean value of 0.025 ± 0.003 s^{-1}. The trapping constants for the high-Cu steel are higher than those for the HRC 53 specimen, whereas the the fluxes tend to be similar for the two steels. Calculated and experimental data for q_a (η = -0.35 V in test 41) were found to agree well, as shown in Figure 23.

Table 9
VALUES OF k_a AND J FOR HIGH-Cu AND HEAT-TREATED 4340 STEEL

Steel	Test	η (V)	E_c (V/SCE)	k_a (s^{-1})	J (nmol cm^{-2} s^{-1})
HRc 53[a]		-0.30	-0.884	0.008	0.07
		-0.35	-0.935	0.007	0.13
Cu	41	-0.25	-0.839	0.026	0.08
		-0.30	-0.891	0.026	0.10
		-0.35	-0.943	0.026	0.12
Cu	42	-0.20	-0.794	0.021	0.06
		-0.25	-0.846	0.034	0.10
		-0.30	-0.898	0.023	0.11
		-0.35	-0.946	0.019	0.11

[a] Data reported previously for 4340 steel HRC 53.

Data for the charge ratios as a function of t_c are shown in Figures 18 and 24. In the case of the high-Cu steel, q_T/q_{in} deviates from a linear dependence on $\sqrt{t_c}$ at long charging

41
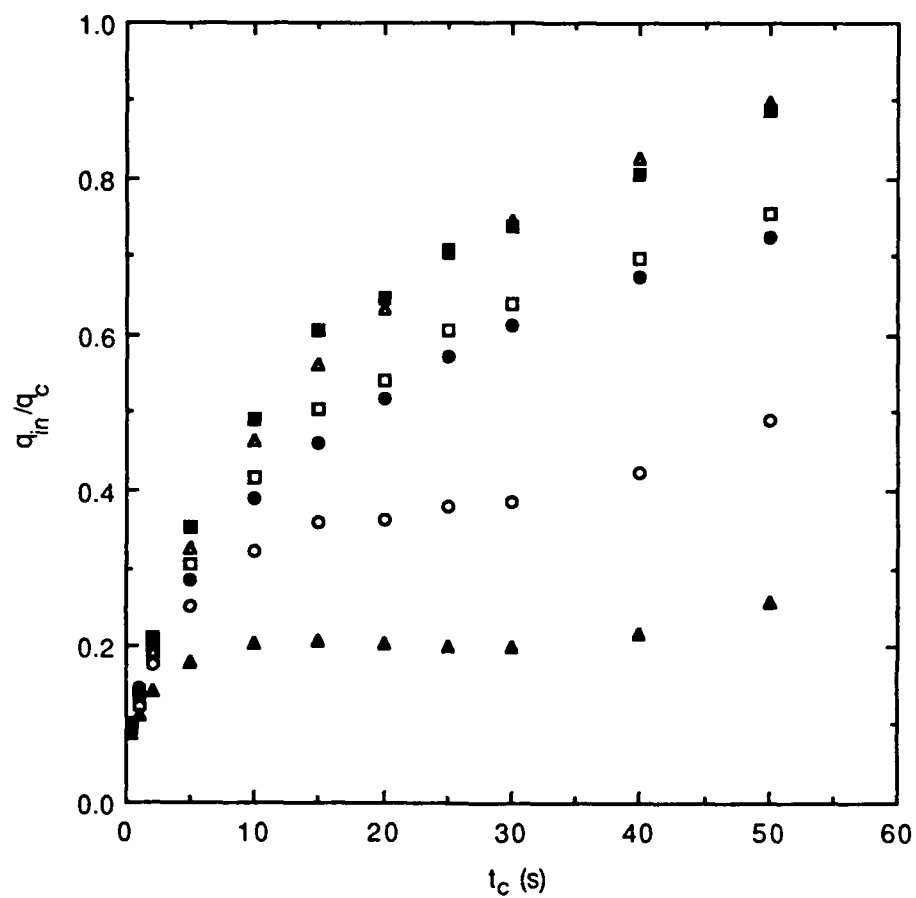
RA-1962-34

Figure 21. Dependence of q_{in}/q_c on charging time for titanium grade 2 at high overpotentials.

□ -0.90 V; ● -0.95 V; ▲ -1.00 V; ■ -1.05 V ;
○ -1.10 V; ▲ -1.15 V.

42
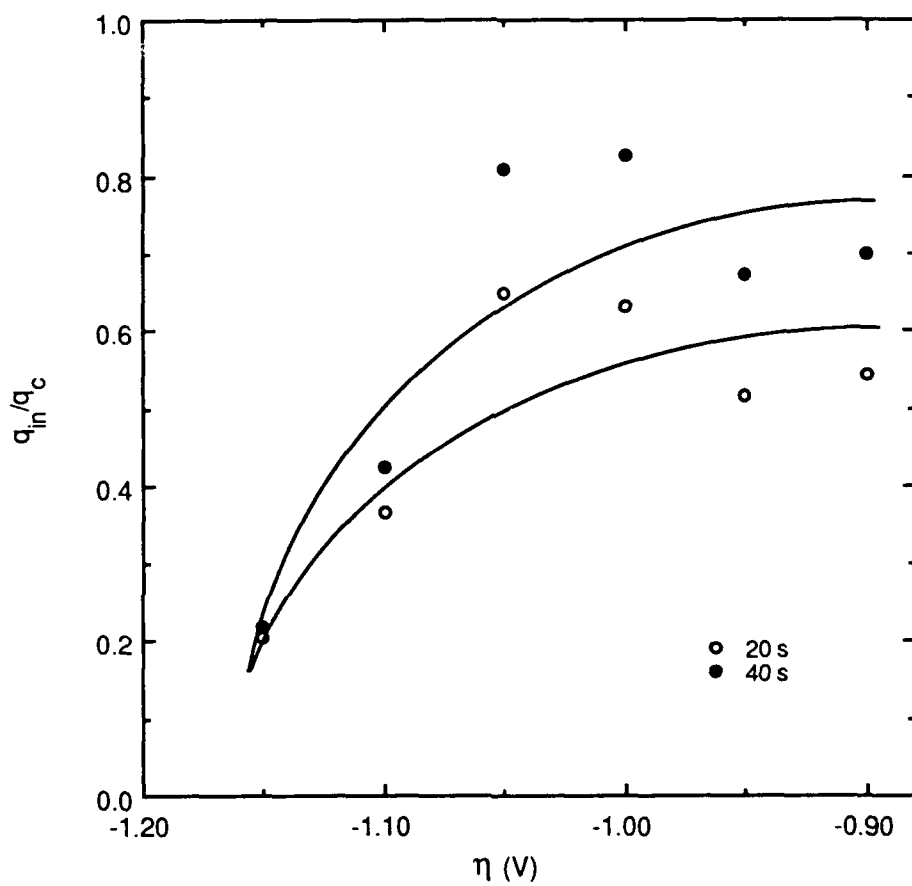
Figure 22. Dependence of q_{in}/q_c on overpotential for titanium grade 2 at high overpotentials and charging times of 20 and 40 s.
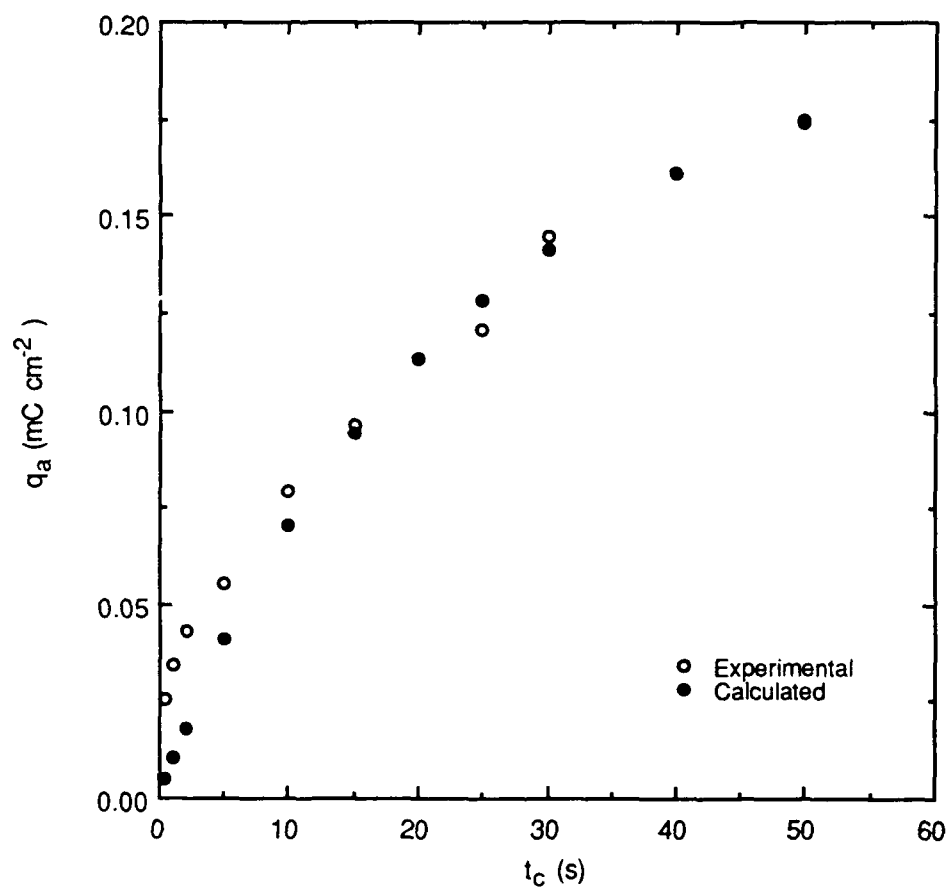
Figure 23. Comparison of experimental and calculated anodic charge
data for high-Cu 4340 steel in acetate buffer.

$E_c = -0.943$ V (SCE).

44
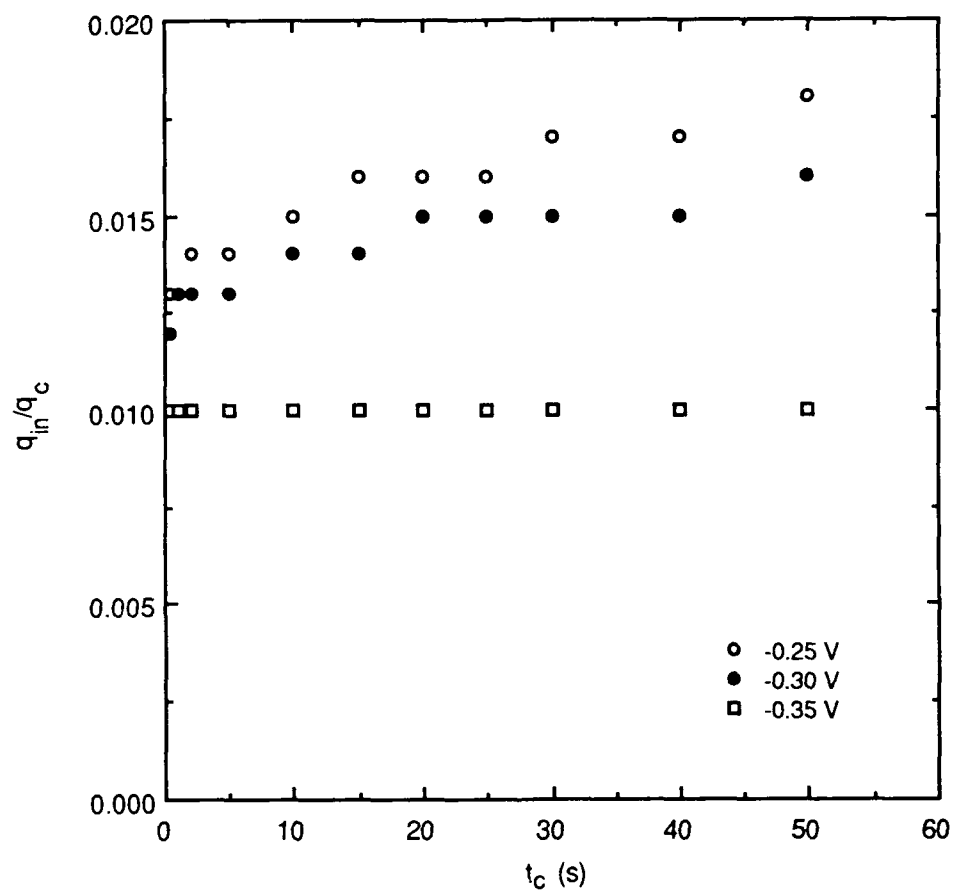
RAM-1962-42

Figure 24. Dependence of q_{in}/q_c on charging time for high-Cu
4340 steel at various overpotentials.

45

times whereas the ratio for the HRC 53 steel is approximately proportional to $\sqrt{t_c}$ over the range studied. The difference in behavior can be attributed to the change in effective trapping by a factor of 3, as indicated by the apparent trapping constants. As with the HRC 53 steel, q_{in}/q_c for the high-Cu alloy shows little or no dependence on t_c. However, q_{in}/q_c for the high-Cu steel does decrease slightly with increasing overpotential, as can be seen in Figure 24, whereas it is independent of overpotential in the case of the HRC 53 steel. Also noteworthy is the difference between the values of q_{in}/q_c for the two specimens; for example, at -0.35 V, q_{in}/q_c for the high-Cu steel is 0.01, compared with 0.02 for the HRC 53 steel.

DISCUSSION

PRECIPITATION-HARDENED ALLOYS

Inconel 718

Irreversible Trapping Constant. The irreversible trapping constant (k) can be derived from k_a by using diffusivity data for the pure Fe-Ni-Cr alloy to obtain D_L and for Inconel 718 to obtain D_a. The minor alloying elements are assumed to be primarily responsible for the reversible trapping behavior in the Inconel because the binding energy of hydrogen to defects such as vacancies or edge dislocations in an fcc lattice is a factor of 4 smaller than the activation energy for diffusion.[13] The apparent diffusivity of hydrogen in Inconel 718 has been measured as a function of temperature from 150° to 500°C and is given (in $m^2 s^{-1}$) by the following equation:[14]

$$D = 1.07 \times 10^{-6} \exp[(-49790 \text{ J mol}^{-1})/RT] \qquad (7)$$

Extrapolation to 25°C gives a value of 2.0×10^{-15} $m^2 s^{-1}$, which is consistent with the diffusivities of other nickel-base alloys at ambient temperature. The most appropriate diffusivity data[15] for the pure Ni-Cr-Fe alloy are for 76% Ni-16% Cr-8% Fe, for which D_L is $(7.9 \pm 1) \times 10^{-15}$ $m^2 s^{-1}$. Although the levels of the three elements, especially Ni and Fe, differ to some extent in the pure alloy and the Inconel, the error in using the diffusivity of the Ni-Cr-Fe alloy for D_L is assumed to be small enough to ignore. Accordingly, by using these data for D_L and D_a, K_r is found to be 3.0 ± 0.5 and, therefore, the value of k is 0.124 ± 0.024 s^{-1}.

Identification of Traps. Previous studies have shown that carbide-matrix interfaces are irreversible traps.[3,16,17] The trapping energy for hydrogen at Fe_3C and TiC interfaces is 77-87 kJ mol^{-1}, which is well in excess of the value of 58 kJ mol^{-1} considered to delineate irreversible and reversible trapping.[3,18] Accordingly, the irreversible traps in Inconel 718 are assumed to be the niobium carbide particles.

47

The density of the irreversible trap particles was calculated from the trapping constant by using Eq. (4). The diameter (a) of the metal atom was taken as the mean of the atomic diameters of Fe (248 pm), Ni (250 pm), Cr (250 pm), and Mo (272 pm) weighted in accordance with the atomic fraction of each element in the alloy. The assumption of a spherical shape is clearly an approximation for carbide particles in the Inconel. However, by using the value of 3.9 μm for the mean radius of the carbide particles, $D_a = 2.0 \times 10^{-15}$ m^2 s^{-1} and $a = 250 \times 10^{-12}$ m, the density of trap particles was calculated as 2.0×10^{13} m^{-3}. The agreement between the actual concentration of carbide particles (2.2×10^{13} m^{-3}) and the trap density is remarkable in view of the assumed spherical shape for the traps and carbides. This close agreement does clearly indicate that large traps with both a high surface area and a high trapping energy can overwhelmingly dominate the irreversible trapping behavior of an alloy.

Incoloy 925

Irreversible Trapping Constant. Evaluation of the irreversible trapping constant (k) from k_a requires diffusivity data for the pure Fe-Ni-Cr alloy to obtain D_L and for Incoloy 925 to obtain D_a. As with Inconel 718, the minor alloying elements are assumed to be primarily responsible for the reversible trapping behavior in the Incoloy. Data are not available for Incoloy 925, but the apparent diffusivity of hydrogen in Incoloy 903 over the temperature range of 150°-500°C is given (in m^2 s^{-1}) by the following equation:[14]

$$D = 2.46 \times 10^{-6} \exp [(-52677 \text{ J mol}^{-1})/RT] \tag{8}$$

Extrapolation to 25°C gives a value of 1.4×10^{-15} m^2 s^{-1}. The most appropriate diffusivity data for the pure alloy are those for the 76% Ni-16% Cr-8% Fe (see Inconel 718 above). The difference in the levels of the three elements between the pure alloy and the Incoloy is larger than that in the case of the Inconel, but in the absence of more appropriate data, the error in using the diffusivity of the Ni-Cr-Fe alloy for D_L must still to be treated as negligible. These data for D_L and D_a were used to obtain a value of 4.6 ± 0.6 for K_r, so k was found to be 0.034 ± 0.004 s^{-1}.

Identification of Traps. Hydrogen-induced fracture in Incoloy 903 is initiated by void formation at matrix carbides.[19] Accordingly, the TiC particles were assumed to

48

provide the irreversible traps in Incoloy 925. The trapping constant for this alloy was used to calculate the density of irreversible trap particles by means of Eq. (4). The diameter (a) of the metal atom in the Incoloy was taken as the weighted mean of the atomic diameters of Fe, Ni, Cr, Mo, and Ti (290 pm). Although the spherical trap shape assumed in deriving Eq. (4) is again somewhat of an approximation for carbide particles in the Incoloy, the carbide particles were assumed to have a mean radius of 1.4 μm. By using $D_a = 2.0 \times 10^{-15}$ m^2 s^{-1} and $a = 250 \times 10^{-12}$ m, the density of trap particles was calculated to be 4.1×10^{13} m^{-3}. The actual concentration of carbide particles (4.6×10^{13} m^{-3}) and the trap density are again in close agreement despite the assumption that the traps and carbides are spherical.

18Ni Maraging Steel

Irreversible Trapping Constant. The mechanical properties and hydrogen permeation parameters for 18Ni maraging steel with a yield strength of 1723 MPa (250 ksi) have been studied as a function of aging temperature.[20] The diffusivity of hydrogen was found to decrease as the aging temperature increases, whereas the hardness increases up to a maximum of about HRC 52 at 500°C and then decreases. The diffusivity for the 18Ni (1723 MPa) steel aged at 480°C is approximately 3.7×10^{-13} m^2 s^{-1}. A comparison[10] with other results indicates that the room temperature diffusivity for hydrogen in maraging steels is between 10^{-12} and 10^{-13} m^2 s^{-1}. The 1723-MPa grade of 18Ni maraging steel nominally contains a little over half as much titanium as does the 2068-MPa (300-ksi) grade, and previous work has shown that the diffusivity of hydrogen in iron is inversely proportional to the titanium content.[10] Therefore, the diffusivity for the 18Ni (nominal 2068-MPa) steel used in this study is assumed to be 1×10^{-13} m^2 s^{-1}, allowing for the higher hardness (HRC 53.8) of this grade.

Diffusivity data for the pure Fe-Ni-Co-Mo alloy are not available. The most appropriate data are those for Fe-Ni alloys,[21] for which D_L (18% Ni) is ~3×10^{-11} m^2 s^{-1} at 27°C. On the basis of previous studies, the difference in diffusivity between Fe-20% Ni and pure iron may be related to trapping effects of the martensitic structure.[10] Accordingly, minor elements, especially Co and Mo, are assumed to have little effect on the diffusivity in the Fe-Ni-Co-Mo alloy. By using the appropriate data for D_L and D_a, K_r was calculated to be 300 ± 90 and therefore $k' = 1.50 \pm 1.05$ s^{-1} and $k'' = 3.0 \pm 2.4$ s^{-1}.

Identification of Quasi-irreversible Traps. The change in k_a between experiments performed 18 hr apart indicates that hydrogen remaining desorbs slowly, which in turn suggests the formation of an unstable hydride during charging. This possibility is consistent with the behavior of Hastelloy C-276, which is known to form an unstable hydride that slowly dissociates over 20 hr at room temperature.[22] Moreover, the C-276 appears to form an alloy hydride rather than NiH.

Potential traps are the intermetallic compounds, Ni_3Mo and possibly Ni_3Ti or FeTi, precipitated during age hardening of the maraging steel.[23] The energy of hydrogen interaction with the intermetallic particles has been estimated at 38.6 kJ mol^{-1}.[24] This value was derived by assuming equilibrium between the traps and lattice but is reasonable when compared with the interaction energies of other metallic traps.[25] The interaction energy for the intermetallics suggests that they are reversible traps, which is perhaps to be expected because reversibility was assumed in the calculation. Nevertheless, these intermetallics must be considered as possibilities for the trap sites from which slow release of hydrogen occurs. Also, the submicroscopic size of the intermetallics would make them likely to be filled during the charging time used in the pulse tests.

The size of the precipitate particles is generally several hundred Angstroms in their largest dimension, and the interparticle spacings are on the order of 300-500 Å.[23] The trap density calculated using these values was 2 x 10^{16} m^{-3}, which is about 5 orders of magnitude lower than the estimated concentration of intermetallic particles. Therefore, the principal quasi-irreversible trap is evidently not a primary or secondary intermetallic precipitate. Rather, these precipitates would appear to be reversible traps, as is implied by the magnitude of their interaction energy.

Another possibility is that the quasi-irreversible trap is associated with microstructural boundaries. Autoradiography studies using tritium have shown that trapping occurs at grain boundaries and martensite boundaries in maraging steel.[26,27] In addition, the location of tritium in the alloy is virtually unchanged after two months except for a small amount of outgassing. Therefore, both sites appear to be moderately strong traps in maraging steel, although grain boundaries are generally considered to be reversible traps in ferritic steels. It is possible that the martensite boundaries are stronger traps than the grain boundaries and so tend more toward irreversibility. If the martensite boundaries as well as the grain boundaries are assumed to have an influence diameter of 3 nm,[25] the trap density is found to be 9 x 10^{17} m^{-3}.

At this stage, the quasi-irreversible trap remains unidentified. A quasi-irreversible trap should have a trapping energy close to the value (58 kJ mol^{-1}) representing the boundary between reversible and irreversible trapping. However, none of the elements in the maraging steel fulfill this requirement. In fact, the trapping energies for most of the atomic traps are well below the range of values for the interfaces and can be treated as reversible.[18,25] Moreover, the density of traps determined from k" by assuming one of the possible atomic traps such as Zr is about 5-6 orders of magnitude lower than the actual number of atoms calculated from the composition of the alloy. Hence, martensite boundaries remain the most likely possibility.

Identification of Irreversible Traps. Intense hydrogen trapping has been observed at carbo-nitride interfaces in maraging steels by using autoradiography[26,27] and indicates Ti(CN) as an irreversible trap in these steels. Accordingly, the density of irreversible traps was calculated using Eq. (4) on the basis of TiC/Ti(CN) particles. The diameter (a) of the metal atom was taken as the weighted mean of the atomic diameters of Fe, Ni, Mo, Ti, and Co (250 pm). The carbide/nitride particles were again treated as spherical, and the trap radius was taken as 1.7 μm. By using $D_a = 2.0 \times 10^{-15}$ m^2 s^{-1} and $a = 250 \times 10^{-12}$ m, the density of the traps was calculated to be 3.4 $\times$ 10^{11} m^{-3}, compared with (1.1 $\pm$ 0.6) $\times$ 10^{13} m^{-3} for the actual concentration of carbide/nitride particles. The two values differ by a factor of ~30, which can be accounted for to a large extent, if not entirely, by the uncertainties in both the concentration of particles and the value of D_a assumed for the 2068-MPa grade of 18Ni maraging steel. In view of these uncertainties, the calculated trap density and the carbide/nitride concentration are considered to correlate moderately well.

WORK-HARDENED ALLOYS

Inconel 625

Irreversible Trapping Constant. Evaluation of k requires diffusivity data for the pure Ni-Cr-Mo alloy to obtain D_L and for Inconel 625 to obtain D_a. As with Inconel 718, the reversible trapping in the 625 alloy is assumed to be associated principally with the minor alloying elements rather than defects such as vacancies or edge dislocations. Data are not available for the pure alloy or Inconel 625. The most appropriate values of D_a and D_L are those for Hastelloy C-276 (see below) and the 76% Ni-16% Cr-8% Fe alloy above,

respectively. While the composition of the pure alloy and the Inconel differ to some degree in the content of their main alloying elements, especially Mo, the error in using the diffusivity of the Ni-Cr-Fe alloy for D_L is assumed to be small. Accordingly, by using D_L = (7.9 ± 1) x 10^{-15} m^2 s^{-1} and D_a = (2.2 ± 0.2) x 10^{-15} cm^2 s^{-1}, K_r is found to be 2.6 ± 0.8 and, therefore, the value of k for Inconel 625 is 0.014 ± 0.010 s^{-1}.

Identification of Traps. The NbTi carbide particles were assumed to act as the principal irreversible traps in Inconel 625. On the basis of this assumption, the density of irreversible trap particles was calculated from the trapping constant for this alloy using Eq. (4). The diameter (a) of the metal atom in the Inconel was taken as the weighted mean of the atomic diameters of Fe, Ni, Cr, and Mo. The carbide particles were again treated as spherical in using Eq. (4) and were considered to have a mean radius of 1.2 μm. By using D_a = 2.2 x 10^{-15} m^2 s^{-1} and a = 251 x 10^{-12} m, the density of trap particles was calculated to be 2.4 x 10^{13} m^{-3}. In view of the uncertainty in D_a for Inconel 625 and the assumption that the traps and carbides are spherical, the trap density is considered to agree well with the actual concentration of carbide particles (7.4 x 10^{13} m^{-3}).

Hastelloy C-276

Irreversible Trapping Constant. The apparent diffusivity of hydrogen in 27% cold-worked Hastelloy C-276 at 25°C was estimated at (2.2 ± 0.2) x 10^{-15} m^2 s^{-1} from data for the annealed and 60% cold-worked forms of the alloy.[28] The most appropriate data for D_L corresponding to the pure Ni-Cr-Mo alloy again are those for the 76% Ni-16% Cr-8% Fe alloy (see above). As with Inconel 625, some compositional differences exist between the pure alloy and Hastelloy but are even more marked in the case of Mo. Nevertheless, the diffusivity for the Ni-Cr-Fe alloy is used for D_L in the absence of more relevant data. By using the appropriate data for D_L and D_a, K_r was calculated to be 2.6 ± 0.8 and, therefore, k' = 0.090 ± 0.030 s^{-1} and k"= 0.068 ± 0.051 s^{-1}.

Identification of Quasi-irreversible Traps. The behavior of k_a is consistent with the formation of an unstable hydride during charging of this alloy, as found by Lunarska-Borowiecka and Fiore.[22] In their work, 2-mm thick specimens were charged at 10 mA cm^{-2} for 20 hr, and X-ray data showed that the hydride disappeared after about 20 hr. In contrast, the hydride formed in the pulse tests evidently dissociated within 1.5 hr, suggesting that it was restricted to small amounts in the surface layer(s) of the alloy in the present case. The decrease in the ingress flux with overpotential observed, for example, in

test 34 is presumably caused by corresponding increases in the amount of hydride formed. The evidence therefore suggests that the apparent rate constant for quasi-irreversible trapping reflects hydrogen trapping via hydride formation. However, although the C-276 is believed to form an alloy hydride, the trap density cannot be determined because of a lack of information on the specific nature of the alloying component involved in the hydride.

Identification of Irreversible Traps. The apparent lack of carbide particles implies that the irreversible traps in this alloy are different from those in the Inconel 625. The susceptibility of Hastelloy C-276 to hydrogen embrittlement has been correlated with the concentration of phosphorus segregated at grain boundaries,[29] so grain boundary phosphorus is assumed to provide the irreversible traps in this case. If hydrogen also segregates to the grain boundaries as in nickel,[30] the grain boundary phosphorus is expected to provide the traps predominantly encountered by the hydrogen.

In earlier work by Mezzanotte et al.[28] on the C-276 alloy, trapping surprisingly appeared to be absent because permeation results failed to show any effect of an increase in the charging potential. The difference in trapping behavior may have been due to differences in the sensitivity between the pulse and permeation techniques or phosphorus levels at the grain boundaries.

The density of irreversible traps was calculated on the basis of atomic phosphorus, using $k_a' = 0.025$ s^{-1} in Eq. (4). The diameter of the metal atom in the Hastelloy was taken as the weighted mean of the atomic diameters of Fe, Ni, Cr, Mo, and W (274 pm). By using $d = 110$ pm, $D_a = 2.2 \times 10^{-15}$ m^2 s^{-1} and $a = 252.5$ pm, the density of irreversible traps was found to be 1.9×10^{22} m^{-3}. The phosphorus content of the alloy was taken as 0.004 wt% (Table 1), which corresponds to a concentration of 8.6×10^{24} atoms m^{-3} that is clearly somewhat greater than the calculated trap density. However, phosphorus at grain boundaries is considered more likely to interact with diffusing hydrogen than that in the bulk alloy and therefore to dominate the irreversible trapping.

Phosphorus in unaged Hastelloy C-276 with a bulk concentration of 0.006-0.008 at% (0.003-0.004 wt%) was previously found to be enriched to 0.3 at% on the surface of grain boundaries.[29] If the surface phosphorus is assumed to lie in the first monolayer and a monolayer is taken as $\sim 10^{19}$ atoms m^{-2}, the surface of the grain boundary is found to contain $\sim 3 \times 10^{16}$ P atoms m^{-3}. An estimate of the amount of grain boundary phosphorus distributed per unit volume of the alloy can be obtained using a simple microstructural model of cubic grains of length b. The number of grain faces per unit volume is $6/b^3$, so

53

the concentration of grain boundaries is $3/b^3$. Therefore, the total grain boundary area per unit volume is $3/b$, and the amount of grain boundary phosphorus per unit volume (C_b) is given by $9 \times 10^{16}/b$ atoms m^{-3}. Mezzanotte et al.[28] determined the grain size for the annealed alloy and found it to vary from 30 to 50 μm. If the grain size for nonannealed C-276 alloy is taken as 5 μm, C_b is found to be $\sim 1.8 \times 10^{22}$ P atoms m^{-3}. The close agreement between the values of C_b and N_i is somewhat fortuitous but demonstrates that it is reasonable to consider phosphorus atoms at grain boundaries rather than in the bulk alloy to be the effective primary irreversible traps.

TITANIUM

Pure Titanium

Titanium in its pure form appears to be resistant to hydrogen penetration. The surface film formed on pure titanium in aqueous solutions is known to be a highly effective barrier to hydrogen entry. Thus, the anodic charge data are consistent with the presence of a hydrogen barrier. Previous work on single crystal TiO_2 in the rutile form[31] has shown that the diffusivity of hydrogen at 20°C is about 4 orders of magnitude higher for the c-axis (1.9×10^{-16} m^2 s^{-1}) than for the a-axis (7.5×10^{-20} m^2 s^{-1}). Therefore, the film orientation can largely determine the resistance of titanium to hydrogen entry, which may account for the difference in charging behavior between the pure and grade 2 forms of titanium.

Titanium Grade 2

Irreversible Trapping Constant. The irreversible trapping constants (k_1 and k_2) for Ti grade 2 can be approximated to the apparent trapping constants on the basis of the low diffusivity of hydrogen in titanium and the closeness in the composition of the grade 2 metal and pure titanium. The diffusivity of hydrogen in α-Ti over the temperature range of 25°-100°C is expressed by

$$D = 6 \times 10^{-6} \exp\left[(-60250 \pm 3347 \text{ J mol}^{-1})/RT\right] \text{ m}^2 \text{ s}^{-1} \tag{9}$$

which gives a value of 1.65×10^{-16} m^2 s^{-1} at 25°C.[32] Because of the diffusivity and composition factors, the diffusivities for the pure and commercial grades are assumed to

differ negligibly, so that $D_a \sim D_L$ and therefore $k = k_a$. Hence, $k_1 = 0.028 \pm 0.002$ s^{-1} and $k_2 = 0.012 \pm 0.006$ s^{-1}.

Identification of Traps. The trapping at low overpotentials as reflected by the value of 0.028 s^{-1} for k_1 could be associated with either the minor elements (C, N, O, and Fe) or structural defects such as grain boundaries and dislocations in the titanium. The density of irreversible traps was calculated from k_1 by assuming that the individual elements were the principal type of trap. The diameter (a) of the titanium atom was taken as 290 pm. The values of N_i and the atomic concentration (A) of the elements are given in Table 10.

Table 10
VALUES OF N_i FOR TITANIUM GRADE 2

Element	d (pm)	N_i (m^{-3})	A (m^{-3})	A/N_i
C	77	6.8×10^{23}	4.8×10^{25}	71
N	74	7.4×10^{23}	1.4×10^{25}	19
O	74	7.4×10^{23}	2.7×10^{26}	365
Fe	124	2.6×10^{23}	8.3×10^{25}	316

The ratio A/N_i represents the level of agreement between the atomic concentration and the trap density calculated on the basis of the appropriate element. In all cases except that of nitrogen, A/N_i is large enough to discount these elements as the principal irreversible trap, even allowing for the uncertainty in the hydrogen diffusivity which could vary N_i by a factor of almost 4. Moreover, oxygen is known to reduce the solubility of hydrogen in titanium,[31] which suggests that oxygen is unlikely to be a potential trap; this finding is consistent with the above results. However, a reasonable correlation exists for nitrogen, particularly because the uncertainty factor means that the calculated trap density may be no more than five times larger than the actual concentration of nitrogen atoms. Interestingly, among the interstitials, nitrogen is particularly effective in reducing the ductility of titanium,[33] which coincides with its apparent role as the principal irreversible trap. Hence,

nitrogen may strongly affect the susceptibility of grade 2 titanium to hydrogen embrittlement through its combined influence on brittleness and hydrogen trapping.

Although the data suggest that the principal irreversible trap may be nitrogen, grain boundaries are another possibility, but in the case of steels, the trapping energy of grain boundaries and therefore their reversible/irreversible nature depend on their angular orientation.[25] A more likely alternative is that trapping results from hydride formation. Hydride decomposition is expected to be slow relative to the duration of a pulse test, and hence the hydrogen can be considered irreversibly trapped.

Previous work has shown that unalloyed titanium absorbs hydrogen in near-neutral brine at 25° and 100°C when the potential is more negative than -0.75 V (SCE).[34] Only thin surface hydride films were found to form at potentials more positive than -1.0 V (SCE), but extensive hydride formation may occur at more negative potentials. Traps corresponding to the formation of a surface hydride could be expected to saturate at potentials approaching the beginning of accelerated hydride formation because of the decreasing availability of free titanium in the vicinity of the surface. Trap saturation would lead to a decrease in k_1 with increasing overpotential, but such a decrease is not observed. Therefore, nitrogen rather than surface hydride formation or grain boundaries seems more likely to act as the principal trap at low overpotentials. The additional trapping constant (k_2) obtained at high overpotentials [E_c <-0.93 V(SCE)] is probably associated with the accelerated formation of hydrides. Moreover, the decrease in q_{in}/q_c in this potential region is consistent with the presence of a partial barrier to hydrogen entry and provides support for the formation of a thick hydride layer.

COPPER-ENRICHED HIGH-STRENGTH STEEL

Irreversible Trapping Constant

The irreversible trapping constant for the Cu-steel can be estimated from k_a using diffusivity data for iron to obtain D_L and for the low Cu-steel to obtain D_a. Previous work has shown that an increase from 0.03 to 0.6% in the copper content of a mild steel in an ASTM solution of pH 5.1 causes only a small decrease in the diffusivity from 1.6×10^{-10} to 1.0×10^{-10} $m^2 s^{-1}$.[35] Therefore, the difference in D_a between 4340 steel with 0.19 and 0.7% Cu is assumed to be insignificant. The most appropriate value available for D_a pertains to HRC 50 electroslag remelted 4340 steel, for which $D_a \sim 10^{-11}$ $m^2 s^{-1}$.[36] The

56

diffusivity for pure iron was taken as 5×10^{-9} m^2 s^{-1}.[37,38] Accordingly, by using these data for D_L and D_a, K_r is found to be 500 and, therefore, the values of k for the Cu-steel and HRC 53 steel are 12.5 ± 1.5 and 4.0 ± 0.5 s^{-1}, respectively.

Effect of Copper

The presence of 0.25-0.3% copper has been reported to eliminate hydrogen-induced cracking in steels,[39] but other work has shown that adding Cu can be detrimental under certain conditions.[35] Several studies have shown that adding copper has a beneficial effect on the basis of reductions observed in ductility loss, blistering and cracking that corresponded to decreases in corrosion rate, and the amount of desorbed hydrogen.[35,40] These results indicated that the presence of copper modifies the alloy surface so as to inhibit the absorption of hydrogen.

The similarity in the hydrogen fluxes for the Cu-steel and HRC 53 steel suggests that a Cu level of 0.19% present in HRC 53 steel is as effective as 0.7% in modifying the surface to reduce hydrogen absorption. On the other hand, the decrease observed in q_{in}/q_c indicates that the increase in copper content renders hydrogen absorption less efficient with respect to charging. However, the values of q_c and the similarity in the fluxes showed that the lower values of q_{in}/q_c for the high-Cu steel are associated primarily with higher cathodic currents rather than with slower hydrogen entry.

Previous workers have reported that additng less than 0.2% Cu has no effect on pipeline steels,[39] but this level can be expected to vary somewhat with the microstructure and, therefore, the type of steel. For example, a semikilled steel with a range of inclusions (Type I MnS, Type I duplex sulfide-silicates and silicates) contained 0.22% Cu but showed extensive blistering and cracking.[39] Hence, the fact that 0.19% Cu is enough to adequately modify the surface of 4340 steel, as indicated by the flux results, appears reasonable in terms of the copper levels required for pipeline steels.

Although the adding copper may reduce hydrogen absorption, the trapping constants indicate that the presence of 0.7% Cu enhances the trapping capability of 4340 steel and therefore is detrimental in raising the susceptibility to hydrogen embrittlement. The increase in trapping is consistent with results from other work on a steel containing 0.03% and 0.6% Cu.[35] In ASTM solutions (pH $\leq$ 2), adding 0.6% Cu reduced both the loss of ductility of the steel and the amount of hydrogen desorbed. However, the observed decrease in desorbed hydrogen could be due to hydrogen trapping as well as to reduced

57

absorption. This factor was underscored by the results for a NACE solution (pH 3). Delayed failure tests showed that adding Cu was detrimental in this case, and the results were consistent with findings of higher hydrogen solubility and lower values of desorbed hydrogen attributed to enhanced trapping. However, in another study,[40] adding 0.28% Cu to a pipeline steel in a NACE solution produced moderate reductions in the corrosion rate and diffusible hydrogen, together with decreases in the blister area and crack length.

Clearly, the effect of copper depends on several factors such as pH and the amount of copper present. The increase in the irreversible trapping constant and the decrease in desorbed hydrogen for 0.6-0.7% Cu suggest that this level renders the steels more susceptible to hydrogen embrittlement, presumably because of the formation of additional traps.

COMPARISON OF TRAPPING PARAMETERS

The mean values of the trapping constants for the nickel-containing alloys and titanium grade 2 are summarized in Table 11. The maraging steel has the highest value of the irreversible trapping constant for these alloys, followed by Inconel 718, the Hastelloy, Incoloy, Ti grade 2, and Inconel 625. The high trapping constant for the steel compared with that for the Inconel is consistent with their relative susceptibilities to hydrogen embrittlement. Previous work on 18Ni (1723 MPa) maraging steel and Inconel 718 subjected to stress-rupture tests during electrolytic charging has shown that the steel undergoes severe embrittlement, whereas the Inconel shows negligible susceptibility.[41,42]

No Incoloys were included in the electrolytic charging tests, but gas-phase charging studies on Incoloy 903 have shown that brief exposure to high-pressure hydrogen is not detrimental, although prolonged exposure, particularly at higher temperatures, can accumulate enough internal hydrogen to reduce ductility.[43] In contrast, gas-phase charging of Inconel 718 causes embrittlement characterized as extreme.[41] These results suggest that Incoloy 903 and, by implication, Incoloy 925 are less sensitive than Inconel 718 to hydrogen embrittlement, so the order of the trapping constants for Inconel 718 and Incoloy 925 evidently parallels their relative susceptibilities to hydrogen embrittlement.

A similar comparison of the susceptibilities of Hastelloy C-276 and Inconel 625 is complicated by their sensitivity to the amount of cold work performed in each case. However, the ranking of these alloys in terms of their resistance to hydrogen embrittlement can be assessed indirectly from previous studies of Hastelloys C-276 and G.[44-46]

Table 11
TRAPPING PARAMETERS

Group	Alloy	k_a (s^{-1})	K_r	k (s^{-1})
Precipitation-hardened	Inconel 718	0.031 ± 0.002	3.0 ± 0.5	0.128 ± 0.024
	Incoloy 925	0.006 ± 0.003	4.6 ± 0.6	0.034 ± 0.004
	Maraging steel	0.005 ± 0.002	300 ± 90	1.50 ± 1.05
		0.010 ± 0.005[a]	300 ± 90	3.00 ± 2.40[a]
Work-hardened	Inconel 625	0.004 ± 0.002	2.6 ± 0.8	0.014 ± 0.010
	Hastelloy C-276	0.025 ± 0.003	2.6 ± 0.8	0.090 ± 0.030
		0.019 ± 0.010[a]	2.6 ± 0.8	0.068 ± 0.051[a]
Titanium	Pure	NA	0	NA
	Grade 2	0.028 ± 0.002	n	0.028 ± 0.002
		0.012 ± 0.006[b]	n	0.012 ± 0.006
4340 Steel	HRC 53	0.008 ± 0.001	500	4.0 ± 0.5
	Cu-enriched	0.025 ± 0.003	500	12.5 ± 1.5

[a]Quasi-irreversible trapping.
[b] Hydride formation.
NA = Not available.

Hastelloy C-276 has a greater tendency to hydrogen embrittlement than Hastelloy G cold-worked to an equivalent degree. The nominal composition of Alloy G is 45Ni-22Cr--6Mo-18Fe-2Co-2Nb-2Cu, which is comparable to that of Inconel 625 in terms of the levels of Cr (22), Mo (8.7), and more important, Nb+Ta (3.5), so it might be expected to be similar in susceptibility to embrittlement. The resistance of Alloy C-276 to embrittlement decreases with an increasing amount of cold work. The Alloy C-276 used in the present study was cold-worked to a greater degree than the Inconel 625 and therefore should be more susceptible to embrittlement, as indicated by the trapping constants. The susceptibility of C-276 relative to the other alloys, as reflected by the position of its trapping constant, is clearly subject to some question because of the uncertainty in the value of k. Moreover, the uncertainty of ±0.030 does not reflect the error involved in using the diffusivity of an Ni-

59

Cr-Fe alloy to obtain D_L in the case of Hastelloy C-276, which contains 16% Mo. Nevertheless, the magnitude of its trapping constant relative to that of Inconel 625 parallels their tendencies to embrittlement.

From the trapping constants for the nickel-containing alloys, the susceptibility of Ti grade 2 to hydrogen embrittlement at low levels of hydrogen is predicted to be similar to that of the Incoloy. Although hydride precipitates can be observed in grade 2 titanium at hydrogen concentrations above ~100 ppm, they do not cause gross embrittlement of the titanium until hydrogen levels exceed 500-600 ppm.[47] Therefore, the similarity in trapping constants for the Incoloy and titanium fits their relative resistance to hydrogen embrittlement in that long exposure times are required for the concentration of hydrogen to exceed the level necessary to result in a loss of mechanical properties. Furthermore, the higher trapping constant (0.040 s^{-1}) associated with the occurrence of significant hydride formation coincides with the increasing susceptibility to embrittlement with hydrogen concentration.

Finally, the irreversible trapping constants for the three nickel alloys and titanium provide an interesting comparison with those obtained earlier[6] for 4340 steel, Monel K-500 (nominally 65Ni-35Cu), and MP35N (nominally 35Ni-35Co-20Cr-10Mo). The values of k for the full range of alloys are listed in Table 12 in descending order. Clearly, there is a strong correlation between the hydrogen embrittlement susceptibility and the trapping capability of the alloy as represented by the irreversible trapping constant. The trapping constants for the three alloys studied earlier fit the overall trend in susceptibility and, as might be expected, indicate that the 4340 steel is the most susceptible, followed by the maraging steel, which has a somewhat lower sensitivity on the basis of its value of k. The sequence of k values for the two steels is in agreement with experimental results which showed that 4340 steel was more susceptible to hydrogen-induced cracking than 18Ni (1723 MPa) maraging steel.[48] At the other extreme, the low trapping constant for MP35N is consistent with the high resistance to hydrogen embrittlement found in practice for this alloy.[49,50]

It is difficult to determine whether the two cold-worked alloys follow the observed pattern for the trapping constants because of a lack of relevant results for hydrogen embrittlement. Moreover, the uncertainty in the values used for D_L to obtain k for Hastelloy C-276 and Inconel 625 compounds the difficulty in evaluating the position of these alloys in Table 12. The main inference that can be drawn from the order of trapping

constants and correlated with data for hydrogen embrittlement is that, as discussed above, the C-276 alloy in this study is somewhat more susceptible to embrittlement than Inconel 625.

The position of Inconel 625 is comparable to that of MP35N within the uncertainty of k. Hydrogen embrittlement of cold-worked nickel-base alloys has been studied as a function of cold reduction (CR) and aging conditions.[49] C-ring specimens galvanically coupled to steel were tested in a NACE solution at different applied stresses. MP35N subjected to 35 and 51% CR and aged at 593°C for 4 hr failed after 21 and <3 days of exposure, respectively, under an applied stress of 100% transverse yield strength, whereas unaged Inconel 625 (59% CR) failed after 11 days. The MP35N specimen used in the trapping studies was obtained as cold drawn rod (1.36 cm in diameter) that had been aged under the same conditions as the C-ring specimens; the amount of cold reduction applied to the rod appears to be in the region of 40-50%.[51] The Inconel 625 with 17% cold work, as used in the present study, should withstand a longer exposure time than that with 59% cold work and therefore be at least as resistant to hydrogen embrittlement as MP35N in a 40% cold reduced and aged condition. In fact, the Inconel may be more resistant than the MP35N specimen, as implied by their different values of k. Hence, the trapping constants of Inconel 625 and MP35N obtained using the pulse technique appear to be consistent with the relative susceptibilities of these alloys to embrittlement.

Table 12
IRREVERSIBLE TRAPPING CONSTANTS

Alloy	Condition	k (s^{-1})
4340 steel	Cu-enriched HRC 53	12.5 ± 1.5 4.0 ± 0.5
18Ni maraging steel	2068 MPa grade	1.50 ± 1.05
Inconel 718		0.128 ± 0.024
Hastelloy C-276	27% Cold work	0.090 ± 0.030
Monel K-500		0.040 ± 0.010
Ti grade 2	High H level	0.040 ± 0.008
Incoloy 925		0.034 ± 0.004
Ti grade 2	Low H level	0.028 ± 0.002
MP35N		0.026 ± 0.002
Inconel 625	17% Cold work	0.014 ± 0.010

CONCLUSIONS

- The ingress of hydrogen in three precipitation-hardened alloys (Inconel 718, Incoloy 925, and 18Ni maraging steel), two work-hardened alloys (Inconel 625 and Hastelloy C-276), and titanium grade 2 was shown to fit a diffusion/trapping model under interface control. Pure titanium does not absorb hydrogen because of the effectiveness of the surface oxide as a barrier to entry.

- Inconels 625 and 718 and Incoloy 925 are each characterized by a single type of irreversible trap. The calculated trap densities indicated that these traps are (NbTi)C, NbTi(CN), and TiC particles, respectively. In contrast, Hastelloy C-276 and 18Ni maraging steel are characterized both by an unidentified quasi-irreversible trap and an irreversible trap thought to be phosphorus segregated at grain boundaries and TiC/Ti(CN) particles, respectively.

- In the case of titanium grade 2, interstitial nitrogen appears to be the principal irreversible trap at low hydrogen levels, although grain boundaries are another possibility. When the concentration of hydrogen becomes high enough, hydride formation provides an additional form of trapping.

- The irreversible trapping constants for the three precipitation-hardened alloys and Ti grade 2 are consistent with their relative susceptibilities to hydrogen embrittlement, with the maraging steel having the highest value, followed by Inconel 718, the Incoloy and Ti grade 2. Moreover, a comparison with 4340 steel and two other nickel-base alloys (Monel K-500 and MP35N) indicates a strong correlation between hydrogen embrittlement susceptibility and trapping capability over the full range of these alloys.

- The two cold-worked alloys also show a relationship between their irreversible trapping constants and relative susceptibilities to hydrogen embrittlement, with Hastelloy C-276 having the higher value of k and being more susceptible to hydrogen embrittlement. The trapping constant of Inconel 625 is comparable to that of MP35N within the uncertainty of the data, suggesting that the two alloys could have a similar resistance to hydrogen embrittlement, in parallel with test results for their cracking susceptibility.

63

- Adding Cu to HRC 53 4340 steel at a level of 0.19% is as effective as 0.7% in modifying the surface to reduce hydrogen absorption. However, although copper may reduce hydrogen absorption, the presence of 0.7% Cu enhances the trapping capability of 4340 steel and therefore renders the steel more susceptible to hydrogen embrittlement, in agreement with results from delayed failure tests.

- The diffusion/trapping model allows a range of microstructural features associated with carbides, hydride formation, and interstitial elements or grain boundaries to be identified as the predominant irreversible traps, either singly or in the presence of multiple principal traps. Moreover, the trapping capability of the individual alloys can be compared to provide a basis for explaining differences in the susceptibility of these alloys to hydrogen embrittlement.

REFERENCES

1. R. Gibala and D. S. DeMiglio, in *Proceedings of the 3rd International Conference on the Effect of Hydrogen on the Behavior of Materials*, I. M. Bernstein and A. W. Thompson, eds. (The Metallurgical Society of AIME, Moran, Wyoming, 1980), p. 113.

2. G. M. Pressouyre and I. M. Bernstein, Metall. Trans. **9A**, 1571 (1978).

3. G. M. Pressouyre and I. M. Bernstein, Acta Metall. **27**, 89 (1979).

4. R. McKibbin, D. A. Harrington, B. G. Pound, R. M. Sharp, and G. A. Wright, Acta Metall. **35**, 253 (1987).

5. B. G. Pound, R. M. Sharp, and G. A. Wright, Acta Metall. **35**, 263 (1987).

6. B. G. Pound, Corrosion **45**, 18 (1989); **46**, 50 (1990).

7. H. L. Eiselstein, "Advances in the Technology of Stainless Steels and Related Alloys," Special Technical Publication No. 369, ASTM (1965).

8. *Inconel alloy 625*, Inco Alloys International (Huntington, West Virginia, 1985).

9. G. F. Vander Voort and H. M. James, in *Metals Handbook*, 9th ed., Vol. 9 (ASM, Metals Park, Ohio, 1987), p. 316.

10. D. P. Dautovich and S. Floreen, in *Proceedings of the Conference on the Stress Corrosion Cracking and Hydrogen Embrittlement of Iron-Base Alloys*, Unieux-Firminy, France (NACE, Houston, Texas, 1973) p. 798.

11. B. G. Reisdorf, Trans. Am. Soc. Met., **56**, 783 (1963).

12. N. T. Thomas and K. Nobe, J. Electrochem. Soc. **117**, 622 (1970).

13. W. D. Wilson and S. C. Keeton, in *Advanced Techniques for Characterizing Hydrogen in Metals*, N. F. Fiore and B. J. Berkowitz, eds., Proc. Symp. AIME, Kentucky (1981), p. 3.

14. W. M. Robertson, Metall. Trans. **8A**, 1709 (1977).

15. M. Cornet, C. Bertrand, and M. Da Cunha Belo, Metall. Trans. **13A**, 141 (1982).

16. W. M. Robertson, Metall. Trans. **10A**, 489 (1979).

17. D. Webster, Trans. TMS-AIME, **242**, 640 (1968).

18. I. M. Bernstein and G. M. Pressouyre, in *Hydrogen Degradation of Ferrous Alloys*, R. A. Oriani, J. P. Hirth, and M. Smialowski, eds., (Noyes Publications, 1985), p. 641.

19. N. R. Moody, M. W. Perra, and S. L. Robinson, in *Proceedings of the 4th International Conference on Hydrogen Effects on Material Behavior* (Moran, Wyoming, 1989).

20. M. T. Wang, Technical Rept. AFML-72-102, Part I (1972); Ref 105 in "The Stress Corrosion and Hydrogen Embrittlement Behavior of Maraging Steels," *Proceedings of the Conference on the Stress Corrosion Cracking and Hydrogen Embrittlement of Iron-Base Alloys*, Unieux-Firminy, France (NACE, Houston, Texas, 1973), p. 798.

21. W. Beck, J. O'M. Bockris, M. A. Genshaw, and P. K. Subramanyan, Metall. Trans. **2**, 883 (1971).

22. E. Lunarska-Borowiecka and N. F. Fiore, Metall. Trans. **12A**, 101 (1981).

23. S. Floreen, Metall. Rev. **13**, 115 (1968).

24. V. I. Sarrak, G. A. Filippov, and G. G. Kush, Phys. Met. Metall. **55**, 94 (1983).

25. M. Pressouyre, Metall. Trans. **10A**, 1571 (1979).

26. P. Lacombe, M. Aucouturier, J. P. Laurent, and G. Lapasset, in *Proceedings of the Conference on Stress Corrosion Cracking and Hydrogen Embrittlement of Iron-Base Alloys*, Unieux-Firminy, France (NACE, Houston, Texas, 1973), p. 423.

27. M. Aucouturier, G. Lapasset, and T. Asaoka, Metallography **11**, 5 (1978).

28. D. A. Mezzanotte, J. A. Kargol, and N. F. Fiore, Metall. Trans. **13A**, 1181 (1982).

29. B. J. Berkowitz and R. D. Kane, Corrosion **36**, 24 (1980).

30. D. H. Lassila and H. K. Birnbaum, Acta Metall. **35**, 1815 (1987).

31. G. R. Caskey, Mater. Sci. Eng. **14**, 109 (1974).

32. I. I. Phillips, P. Poole, and L. L. Shreir, Corros. Sci. **14**, 533 (1974).

33. A. E. Jenkins and H. W. Worner, J. Inst. Metal. **80**, 157 (1951/52).

34. H. Satoh, T. Fukuzuka, K. Shimogori, and H. Tanabe, in *Proceedings of the 2nd International Congress on Hydrogen in Metals* (Paris, 1977).

35. G. Philipponneau, M. Habashi, J. Galland, and P. Azou, in *Proceedings of the 1st International Conference on Current Solutions to Hydrogen Problems in Steels*, C. G. Interrante and G. M. Pressouyre, eds. (ASM, Metals Park, Ohio, 1982), p. 168.

36. J. A. Kargol and L. D. Paul, in *Proceedings of the 1st International Conference on Current Solutions to Hydrogen Problems in Steels*, C. G. Interrante and G. M. Pressouyre, eds. (ASM, Metals Park, Ohio, 1982), p. 91

37. R. A. Oriani, Acta Metall. **18**, 147 (1970).

38. A. J. Kumnick and H. H. Johnson, Metall. Trans. **5**, 1199 (1974).

39. E. M. Moore and J. J. Warga, Mater. Perform. **15**, 317 (1976).

40. T. Taira, K. Tsukada, Y. Kobayashi, H. Inagaki, and T. Watanabe, Corrosion **37**, 5 (1981).

41. R. J. Walter, R. P. Jewett, and W. T. Chandler, Mater. Sci. Eng. **5**, 98 (1969/70).

42. T. P. Groeneveld, E. E. Fletcher, and A. R. Elsea, "A Study of Hydrogen Embrittlement of Various Alloys," Summary Report, Contract No. NAS8-20029, NASA, MSFC, Huntsville, Alabama (1966).

43. C. G. Rhodes and A. W. Thompson, Metall. Trans. **8A**, 949 (1977).

44. N. Sridhar, J. A. Kargol, and N. F. Fiore, Scripta Met. **14**, 1257 (1980).

45. R. J. Coyle, Jr., J. A. Kargol, and N. F. Fiore, Metall. Trans. **12A**, 653 (1981).

46. J. A. Kargol and B. Ladna, Scripta Met. **16**, 191 (1982).

47. R. W. Schutz and D. E. Thomas, in *Metals Handbook*, 9th ed., Vol. 13 (ASM, Metals Park, Ohio, 1987), p. 669.

48. T. P. Groeneveld, E. E. Fletcher, and A. R. Elsea, "A Study of Hydrogen Embrittlement of Various Alloys," Technical Support Package to NASA Tech. Brief No. 67-10141, NASA, Washington D.C. (1967), p. 135.

49. R. D. Kane, M. Watkins, D. F. Jacobs, and G. L. Hancock, Corrosion **33**, 309 (1977).

50. J. P. Stroup, A. H. Bauman, and A. Simkovich, Mater. Perform. **15**, 43 (1976).

51. *Multiphase MP35N Alloy Technical Data*, Latrobe Steel Company (Latrobe, Pennsylvania, 1980).

APPENDIX

SURFACE FILMS ON NICKEL-BASE SUPERALLOYS

INTRODUCTION

Superalloys are frequently used in applications where high strength and corrosion resistance are required. As with other corrosion-resistant alloys, the ability of superalloys to withstand aggressive environments depends on the nature of the passive film on the alloy surface. The oxide formed on Inconel 625 in aerated nitric acid solution has been studied[1] by Auger electron spectroscopy (AES), which showed that the film in the passive region contains primarily nickel and chromium with little molybdenum. The passive films formed on three Fe-Cr-Ni alloys (AISI 304 stainless steel, Incoloy 800, and Inconel 600) in alkaline environments have been studied and relative enrichments or depletions of the alloying constituents (Fe, Cr, and Ni) were detected in the surface layers of the films.[2] However, in general there appears to have been little attempt to investigate the surface films formed on superalloys in aqueous environments.

The surface films formed on alloys not only provide high corrosion resistance but also act as a barrier to hydrogen ingress. The film can reduce the rate of hydrogen entry into the metal and inhibit the kinetics of hydrogen formation from reduction of H^+ or H_2O. Thus, the lower entry flux can arise from either a lower surface coverage of adsorbed hydrogen, resulting from slower kinetics of H^+/H_2O reduction, or a low rate constant for the transfer of adsorbed hydrogen into the oxide.

The presence of a surface oxide can in principal affect the analysis of hydrogen ingress data using the diffusion/trapping model because the model implicitly assumes that the oxide thickness constitutes only a very small (preferably negligible) fraction of the total diffusion distance traversed by the mobile hydrogen.

In view of these factors, the composition and thickness of the passive film on three nickel-base superalloys (Inconel 718, Incoloy 925, and MP35N) were investigated in relation to the effect of the films on both the corrosion resistance and hydrogen ingress. The films were studied using a new analytical technique known as surface analysis by laser ionization (SALI).[3,4] This technique was previously applied in a study of passive films on dilute binary alloys (Ni-xAl, Ni-xTi, and Ni-xMo, where x = 0.1 to 8 wt%)[5] and has now been extended to more complex engineering alloys.

EXPERIMENTAL PROCEDURE

Previous studies of passive films have involved techniques such as secondary ion mass spectrometry (SIMS), X-ray photoelectron spectroscopy (XPS or ESCA) and AES. However, SIMS is sensitive to matrix effects so that the observed response can vary greatly depending on the local chemical matrix. As a result, calibration with standards of similar structure and composition is required to determine the composition of the sample quantitatively, but such standards are usually inappropriate for very thin films and interfaces. AES and XPS are much more quantitative than SIMS, but their sensitivity is rather limited, hydrogen cannot be detected, and the depth resolution is somewhat less than that for sputtering techniques because of the electron escape depth.

In contrast, SALI has the ability to perform in-depth and laterally resolved chemical composition measurements quantitatively and with a sensitivity comparable to that of SIMS, but without being greatly susceptible to matrix effects. The depth resolution and limits of detection for SALI exceed those for AES and XPS. The quantitative analysis of specimens using SALI has been treated previously,[3,4,6-9] and SALI was found, for example, to be quantitatively much more accurate than SIMS in studies of contaminated GaAs[6] and fluorine implanted in Si/SiO_2.[7] On the basis of these characteristics, SALI was an attractive technique to use for determining the composition profile in passive films on alloys containing multiple elements.

The composition of each alloy is given in Table A-1. Test specimens of each alloy were prepared as 0.2-cm thick disks cut from the 1.27-cm diameter rods supplied for the hydrogen ingress study. The disks were polished on both sides with SiC paper, followed by 0.05-μm alumina powder on the side that was to be examined using SALI. The passive film was formed by exposing the specimens for 1 hr in the deaerated acetic acid/sodium acetate (15 ppm As_2O_3) solution at $22° \pm 2°C$. After exposure, the alloy samples were washed with distilled water, dried, and immediately transferred to the vacuum sample chamber of the SALI mass spectrometer.

The operation of SALI has been described in detail elsewhere.[3,4] Briefly, the analysis of the sample consists of three steps performed under vacuum: (1) stimulated desorption of neutral atoms and molecules, (2) nonselective photoionization, and (3) reflecting time-of-flight (TOF) mass spectrometry. Because neutrally charged species constitute the vast majority of desorbing particles, this neutral component rather than desorbed ions is examined, thereby allowing semiquantitative experimental data to be

acquired without using standards. Quantitative information can be obtained with a standard or calibrant that need not be especially closely matched to the sample. This latitude is particularly advantageous in analyzing very thin films and interfaces for which closely matched standards generally cannot be found. In the case of SALI, the composition of the film can readily be determined quantitatively from the experimental data by using the bulk concentrations of the alloys themselves as convenient internal standards.

Table A-1
ALLOY COMPOSITION (wt %)

Element	Inconel 718	Incoloy 925	MP35N
Al	0.60	0.30	
B	0.003		
C	0.03	0.02	0.003
Co	0.16		33.15
Cr	18.97	22.20	20.19
Cu	0.04	1.93	
Fe	16.25	28.96	0.34
Mn	0.10	0.62	<0.01
Mo	3.04	2.74	9.55
Ni	54.41	40.95	35.88
P	0.009		0.003
S	0.002	0.001	0.002
Si	0.11	0.17	0.02
Ti	0.98	2.11	0.85
Nb+Ta	5.3		

Desorption for SALI is achieved with ions, electrons, or laser beam or, thermally, with ions typically being used for sputtering in inorganic material analyses. Information about composition as a function of depth can be obtained using the ion beam for milling the sample, often with depth resolutions of 25 Å after 1000 Å of sputtering and a few angstroms near the surface. Preferential sputtering can affect the quantitative analysis of

films for depth-profiling surface techniques in general, but any effect is expected to be similar for the three high-nickel alloys used in this work.

Nonresonant multiphoton ionization was used in this study and is induced by using intense, focused, and pulsed UV laser light. The wavelength and power of the light for this work were 266 nm and ~15 mJ/pulse, respectively. Intense, focused, and pulsed laser light will often produce saturation ionization within the laser focal volume for one- and two- photon processes.[3,8,9] Because the elements of interest in this work ionize with two photons, the ionization efficiency should be nearly the same for these species. Moreover, high sensitivity is obtained by operating under conditions of saturation ionization. With nonresonant multiphoton ionization, the oxidation state of species within the film cannot be determined, but this aspect is expected to be amenable to analysis by using single-photon ionization in future studies.

The relative intensities of the different species were determined for various depth points through the film and alloy. In this study, the surface films were sputtered using a 7-keV Ar^+-beam incident at 60° from normal to the surface. The beam was rastered over an area of 1 mm^2 and had a sputter rate (cm^2 s^{-1}) of 3.4 x 10^{13} Y, where Y is the sputter yield. The value of Y for a 7-keV beam normal to the surface is ~4 for stainless steels, iron, and nickel[10] and is assumed to be 4.0 ± 0.5 for the three high-nickel alloys. Accordingly, for the Ar^+-beam at 60°, the sputter rate is estimated at (2.7 ± 0.3) x 10^{14} cm^{-2} s^{-1}.

Sputtering, of course, is statistical and not absolutely uniform, but with this caveat we estimated the above sputter rate to be equivalent on average to about 0.27 monolayer s^{-1} on the basis that 1 monolayer contains ~10^{15} atoms cm^{-2}. The sputtering time for each depth point is 5 s, so ~1.35 monolayers are removed during this time. Fifty spectra were obtained from the sputtered layer for each depth point and integrated to provide an overall spectrum for the particular point. Accordingly, the composition reflected by the overall spectrum is assumed to correspond to a point midway through the layer, so each depth point represents a cumulative depth of 0.675(2n - 1) monolayers, where n is the depth point number. The actual sputter depth through the oxide was estimated by taking 1 monolayer as half the lattice constant for NiO (4.18 Å) and therefore is given by (0.14 ± 0.02)(2n - 1) nm.

RESULTS

The position of the oxide-alloy interface could not be determined from the depth profiles for atomic oxygen because of noise in the mass spectra, given the limited power of the laser available for the study. However, depth profiles of the ^{68}CrO diatomic molecule provided a suitable oxygen marker and were used to obtain the position of the oxide-alloy interface (Figures A-1 to A-3). The CrO profiles are similar for the three alloys, with the relative intensity (I) showing a sharp maximum before becoming constant within the noise level at about 6 ± 1 depth points, which was assumed to represent the boundary between the oxide and alloy. The position of the boundary did not appear to differ appreciably between the alloys; that is, the three oxides were similar in thickness, which was estimated for 6 depth points to be approximately 1.5 ± 0.5 nm.

Atomic concentration ratios given by c(M)/c(Ni), where M is an alloying element, were calculated from the corresponding spectral intensity data [I(M)/I(Ni)] using the known compositions of the bulk alloys as standards. Contributions to the total concentration of M from molecular species, such as CrO in the case of Cr, were small compared with the primary metal photoion and could be ignored. Nickel was used as the base for the ratios because it is a major component of all three alloys studied. The composition of the metal component in the oxides was determined from the concentration ratios and represented in terms of the concentration (A in atomic percent) of each contributing element in the metal component.

Depth profiles for each alloy are shown in Figures A-4 to A-6. In general, only the principal alloying elements are shown for clarity. However, a more detailed composition of the metal component in the near surface layer of the oxides is given in Table A-2. These data show that the outer surface layer of the film on the Inconel is primarily a Ni-Cr-Fe oxide with only a small amount of Mo present. The Incoloy appears to form a more complex Ni-Fe-Cr-Cu oxide in which the copper and iron are present at similar levels. A feature of this oxide is the high Cr content (49%) of the metal component compared with that (37%) of the Inconel oxide. In the case of MP35N, the film is basically an Ni-Cr-Co oxide but contains somewhat more Mo than is found with the other two alloys.
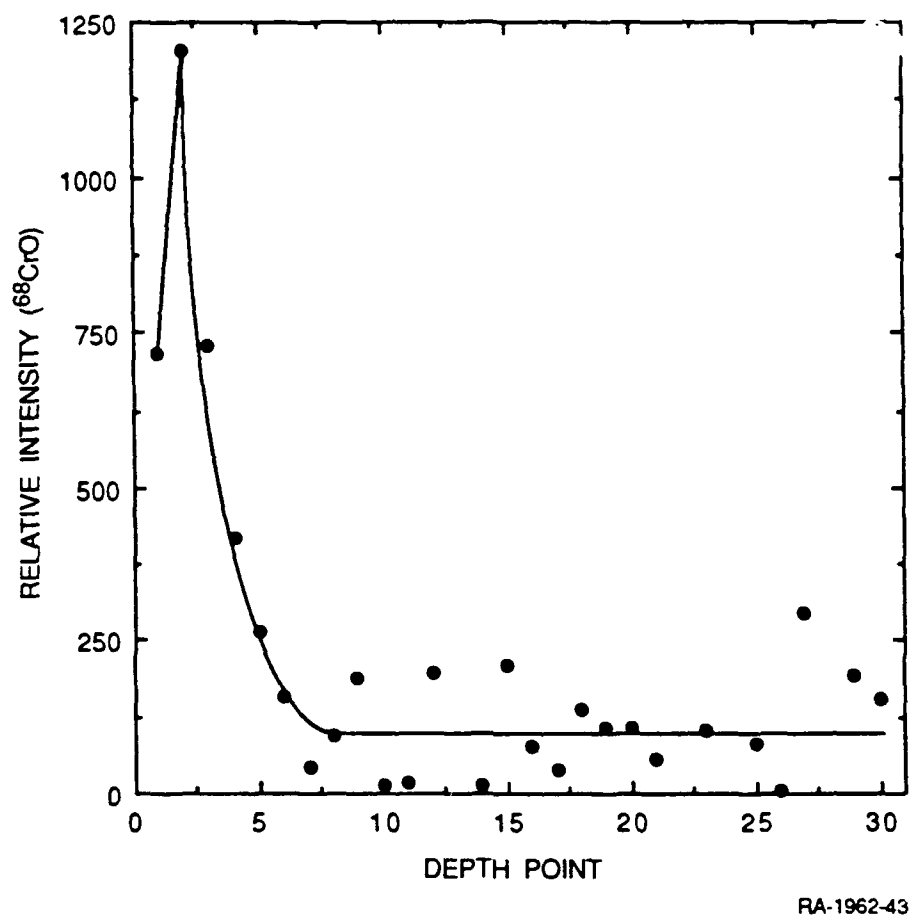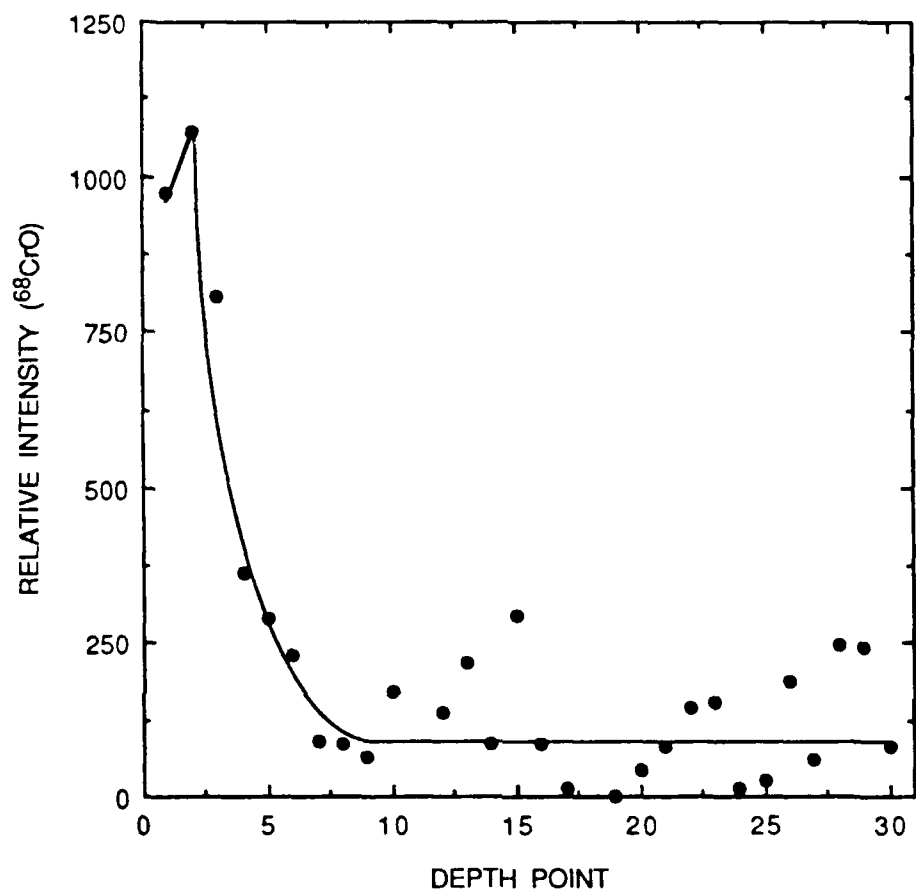
RA-1962-43

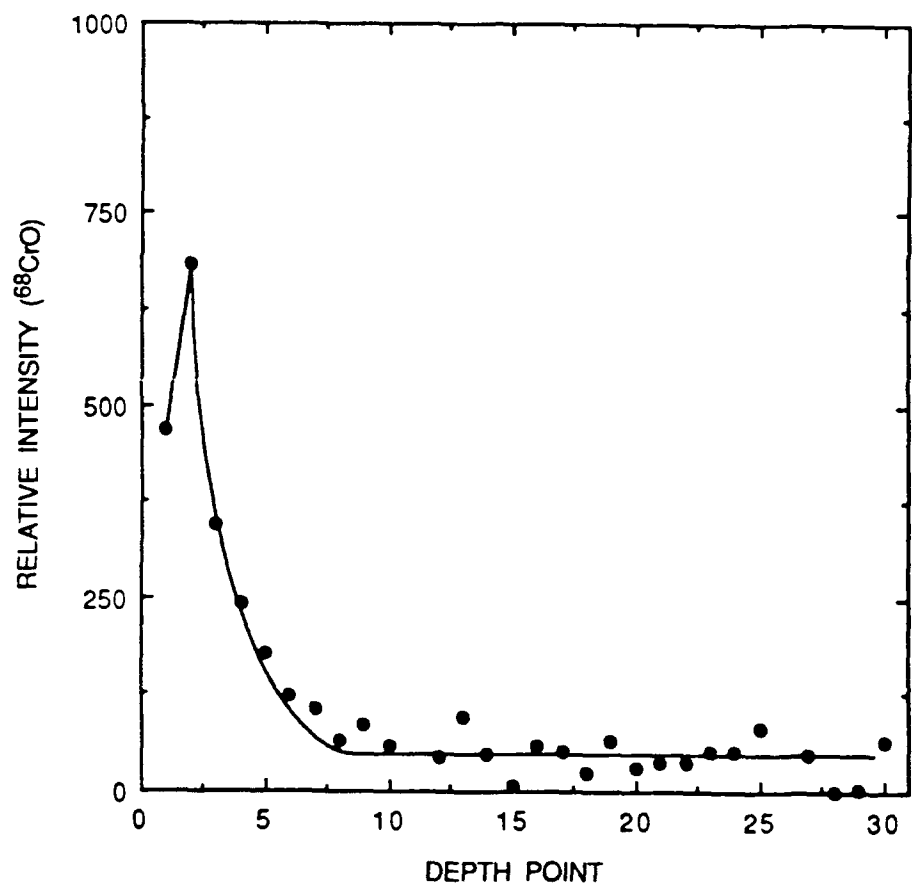Figure A-1. Concentration profile of ^{68}CrO for Inconel 718.

Figure A-2. Concentration profile of ^{68}CrO for Inconel 718.

RA-1962-44

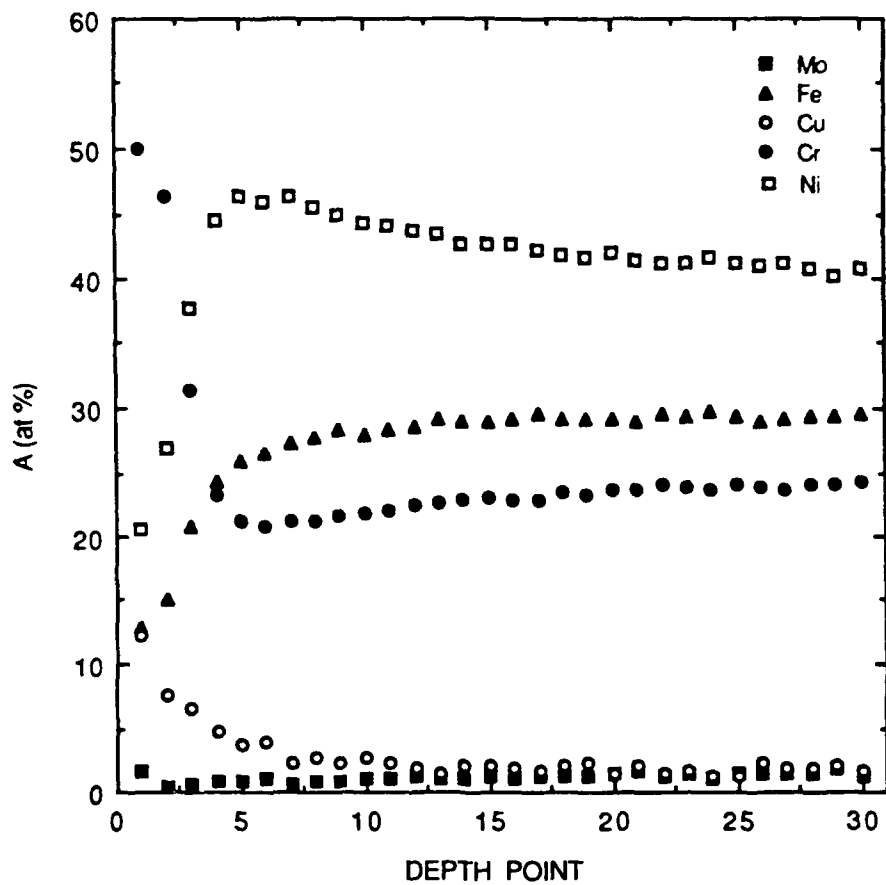RA-1962-45

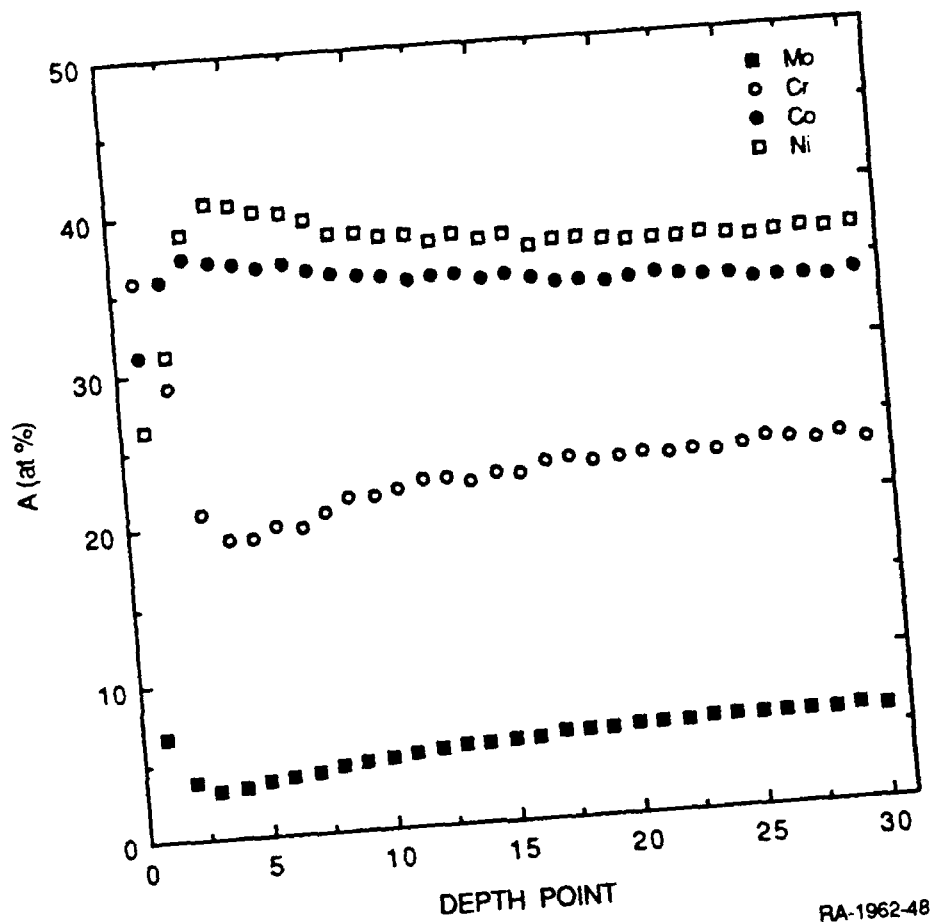Figure A-3.   Concentration profile of ^{68}CrO for Inconel 718.
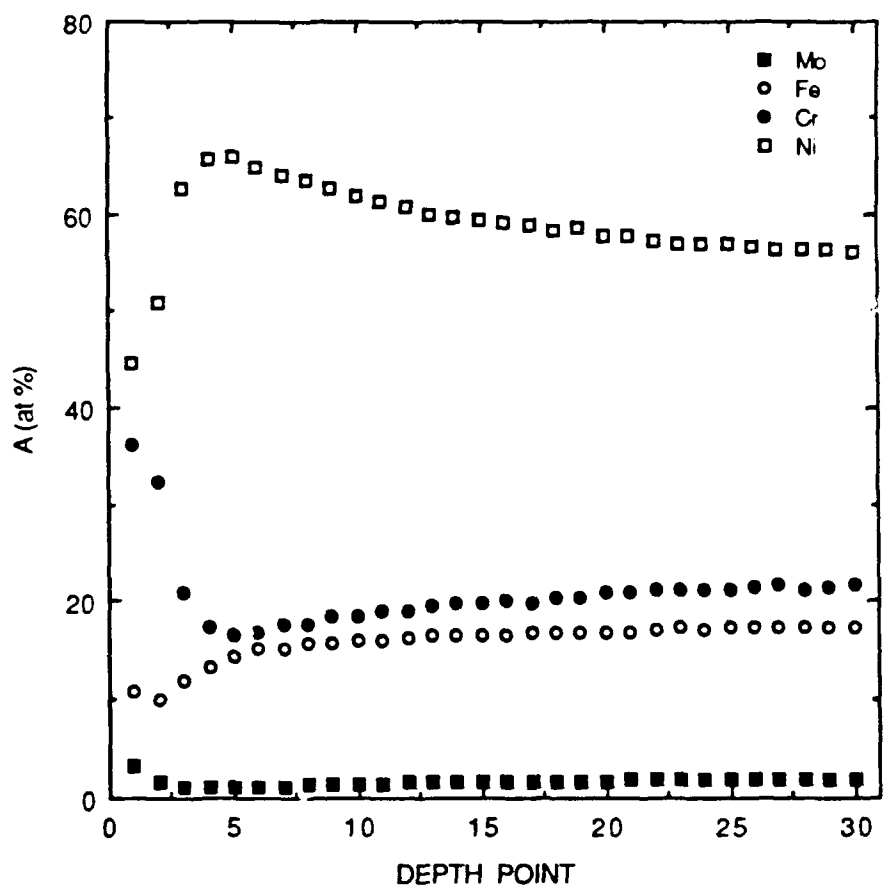
RA-1962-46

Figure A-4. Atomic composition profile of metal component for
Inconel 718.

RA-1962-47

Figure A-5. Atomic composition profile of metal component for
Incoloy 925.

Figure A-6. Atomic composition profile of metal component for MP35N.

RA-1962-48

Table A-2
RELATIVE CONCENTRATIONS OF ELEMENTS

Alloy	Element	Alloy A_{alloy} (at%)	Alloy c(M)/c(NI)	Near-Surface Oxide c(M)/c(NI)	Near-Surface Oxide A_{film} (at%)	EF[a]
718	Cr	21.9	0.394	0.814	36.2	1.7
	Fe	17.5	0.315	0.245	10.9	0.6
	Mo	1.9	0.034	0.075	3.3	1.8
	Nb[b]	1.7	0.031	0.088	3.9	2.3
	Ti	1.2	0.022	0.025	1.1	0.9
	Ni	55.6	1.000	1.000	44.5	0.8
925	Cr	24.5	0.614	2.422	49.9	2.0
	Fe	29.7	0.744	0.622	12.8	0.4
	Mo	1.6	0.040	0.084	1.7	1.1
	Cu	1.7	0.043	0.592	12.2	7.2
	Ti	2.5	0.063	0.131	2.7	1.1
	Ni	39.9	1.000	1.000	20.6	0.5
MP35N	Cr	23.4	0.636	1.358	35.8	1.5
	Mo	6.0	0.163	0.253	6.7	1.1
	Co	33.9[c]	0.921	1.186	31.2	0.9
	Ni	36.8	1.000	1.000	26.3	0.7

[a] EF = enrichment factor.

[b] Nb was assumed to comprise half the Ta+Nb content.

[c] This value has an uncertainty of ±10% because of the Co signal reaching saturation; the resulting error in the atomic composition of the oxide is 8% (±2.4) for Co and 3% (≤1.2) for the other elements.

Comparison of the metallic composition data shows the effect on the oxide of differences in composition between the two iron-containing alloys. The increase in the Fe content from the Inconel to the Incoloy results in a smaller proportional increase for the oxides. However, the decrease in the atomic levels of Ni and Mo between the 718 and 925 alloys is magnified in the oxide. Likewise, the small differences in the Cr and Ti content of the alloys are enhanced in the oxide. Clearly, changes in the alloy composition tend to produce more pronounced changes in the oxide, reflecting the strong segregating influence of the films.

These effects can be examined more quantitatively in terms of enrichment factors (EF) defined by the ratio A_{film}/A_{alloy} (Table A-2). For all three alloys, the EF values are significantly higher than 1 for chromium, indicating marked enrichment of the oxides by

this element, whereas the oxides are evidently depleted in nickel and iron (where relevant) compared with the alloys. In the case of the Inconel and Incoloy, EF is 1.7 and 2.0 for Cr, respectively, but ≤0.8 for Ni and ≤0.6 for Fe, illustrating the degree to which the oxides are enriched in Cr. Also, the respective oxides undergo considerable enrichment in Nb and Cu. In fact, copper segregates to such an extent for Incoloy 925 that it is one of the four principal elements in the metallic component of the oxide but only a minor element in the alloy itself. Interestingly, Ti tends to segregate to the oxide on the Incoloy but is slightly depleted in the case of the Inconel.

The EF values show marked differences in enrichment between the Inconel and Incoloy for each element and highlight the variations in oxide composition with different alloys. For example, in the case of Cr, the higher EF value for the Incoloy shows the disproportionately large change induced in the oxide by the higher level of this element in the alloy compared with that in the Inconel. In contrast, the Inconel shows higher enrichment factors for Mo and Ni than the Incoloy, indicating greater segregation of these elements to the oxide on the Inconel. The alloying elements in MP35N follow trends in enrichment similar to those for the Inconel but to a lesser degree, particularly in the case of Mo.

DISCUSSION

The oxides formed on the three alloys are characterized by a high chromium content because of the marked segregation of this element to the film. Chromium enrichment has also been observed in films on other alloys and appears to be a general phenomenon for passive oxides. In studies using AES, the films on stainless steels,[11] Fe-Cr alloys,[12] Fe-Cr-Mo alloys,[13] and Inconels 625[1] and X-750[14] were all found to be considerably enriched in chromium. In addition, the chromium enrichment observed for the three alloys in this study was accompanied by a depletion in nickel that has also been found to occur for Inconel X-750.

Molybdenum enrichment appears to depend on the particular alloy. The EF values in Table A-2 indicate that the oxides on Incoloy 925 and MP35N are only slightly enriched, whereas considerable enrichment occurs with Inconel 718. An AES study of Fe-17Cr-xMo (x = 1, 3, and 7 wt%) found the Mo content of the passive film to be the same as that in the alloy.[13] However, studies of molybdenum enrichment in stainless steels have provided conflicting results.[15] In work using AES, enrichment of Mo with mill-finished Types 304 and 316 stainless steels was observed in one case.[16] In contrast, other AES

studies indicated that adding Mo to the alloy enhanced only Cr enrichment and that Mo was present in a small amount midway through the film but not on the surface or in the near surface layer.[11,17] However, other work using ESCA found that Cr enrichment was not enhanced by Mo.[18]

Incoloy 925, with its higher Fe, lower Ni content compared with that of Inconel 718, would be more likely to show film characteristics similar to those of the stainless steels and Fe-17Cr-xMo alloy. The SALI data for Incoloy 925 are, in fact, essentially consistent with the results for both the Fe-17Cr-xMo alloy and generally the stainless steels in terms of the lack of Mo enrichment. In contrast, the Inconel shows a different behavior that is probably related to its higher Ni, lower Fe content. Accordingly, the effect of Mo on Cr enrichment should be treated circumspectly in comparing the Incoloy and Inconel, perhaps more so because the EF values suggest that an increase in Mo concentration for the alloy is accompanied by a diminished Cr enrichment; this decrease is in contrast to the results for the stainless steels, which showed either no change or an increase in enrichment for Cr.

Interestingly, MP35N has a similar Ni content to that of the Incoloy and also shows only a slight enrichment of Mo, suggesting that the level of Ni rather than Fe has an influence on Mo segregation. On this basis, the dilute binary Ni alloys analyzed previously[5] using SALI would be expected to show a marked enrichment of Mo in the oxide. Such an enrichment was observed, providing further evidence of a relationship between Mo segregation and Ni content.

The composition of the oxide on Inconel 718 showed some interesting correlations with that grown on Inconel 625 in aerated nitric acid solution (pH 3.7).[1] The passive films on both alloys contain primarily Ni and Cr with little molybdenum. Moreover, the low level of Fe (10.9 at% of the total metal component) in the oxide on the 718 alloy is consistent with the lack of any Fe detected in the film on Inconel 625. This work showed that the decrease in iron content from Incoloy 925 to Inconel 718 was reflected by a decrease in the respective oxides. Therefore, the lower iron content of Inconel 625 (3.8 wt%) compared with that for Inconel 718 and Incoloy 925 (16.25 and 28.96 wt%, respectively) could be expected to result in essentially an Fe-free oxide.

The marked differences in the composition of the oxides in this work have implications for the corrosion performance of the three alloys. The combination of a high Cr and high Mo content in the oxide on MP35N would be expected to render this alloy extremely corrosion-resistant, which is in fact observed experimentally.[19] The oxide on

Inconel 718 is presumed to contain a lower Mo concentration than that on MP35N in accordance with the composition of the metal component in the two films. However, the effect of the lower Mo concentration on the corrosion resistance of Inconel 718 should be offset to some extent by the enrichment of Nb; as an individual element, Nb behaves as an ideal valve metal and so could be expected to promote a barrier type of passive film on the alloy. Indeed, Nb has been found to stabilize the passive film on a ferritic stainless steel (Fe-26Cr) in sulfuric acid.[20]

In the case of Incoloy 925, the considerable enrichment of Cu in the oxide may likewise be beneficial to the corrosion resistance, although there is conflicting evidence of its effect on the corrosion resistance of stainless steels. Adding Cu has been found to increase the corrosion resistance of an austenitic stainless steel (Fe-18Cr-8Ni)[21] but has a detrimental effect on the passivity of the Fe-26Cr ferritic alloy.[20] If Cu does improve the stability of the passive film on the Incoloy, it may be more by affecting the Ni-Fe balance in the film rather than by directly enhancing the protective nature of the oxide.

Besides their effect on corrosion resistance, the surface oxides can influence hydrogen ingress into the alloys in terms of both the absorption and subsequent diffusion of hydrogen. The effect on diffusion depends on the film thickness. The use of a potentiostatic pulse technique in conjunction with a diffusion/trapping model in recent studies of hydrogen ingress into film-covered alloys was based on the assumption that the oxide thickness is a negligible fraction of the total diffusion distance; that is, the principal effect of the oxide is to reduce the absorption of hydrogen into the alloy. If the oxide is thin enough, it can be shown, as follows, that essentially the full distance of hydrogen diffusion does lie in the metal phase at least for the three alloys in this work.

The mean distance of hydrogen diffusion (assuming that diffusion occurs without interference) can be estimated by

$$\chi = (2D_L t_c)^{1/2} \tag{A-1}$$

where D_L is the lattice diffusivity and t_c is the time during which the alloy is charged with hydrogen. On the basis of the limited data available for the diffusivity of hydrogen in oxides,[22] the value of D_L for the oxides on nickel-base alloys is assumed to be $\leq 10^{-17}$ m^2 s^{-1}. Hence, the time required for hydrogen to penetrate a 1.5 nm-thick film is ~0.1 s. In contrast, the potentiostatic pulse data were analyzed for charging times of 10-50 s, so

diffusion through the oxide involves ≤1 % of the total time for hydrogen ingress. The diffusivity of hydrogen in nickel-base alloys is typically on the order of $10^{-15} \text{ m}^2 \text{ s}^{-1}$. Therefore, if the remaining time is assumed to be available for diffusion through the alloy in accordance with Eq. (A-1), the depth of hydrogen penetration in the alloy is found to range from 0.14 to 0.32 μm for charging times from 10 to 50 s. Hence, the film represents only about 0.5-1% of the total diffusion distance in the nickel-base alloys. Although these values are only estimates, they do support the assumption implicit in using the pulse technique that the film is a negligible part of the overall distance traversed by hydrogen.

CONCLUSIONS

The technique of surface analysis by laser ionization was used to determine the nature of the oxide films formed on three nickel-base superalloys (Inconel 718, Incoloy 925, and MP35N). The composition profiles obtained for the passive films by this technique showed the following features:

- The films on all three alloys were enriched in Cr but were depleted in Ni and Fe (where relevant). Mo enrichment occurs with the Inconel but only slightly with MP35N and the Incoloy. The degree of enrichment by each element differs significantly between the alloys. Cr enrichment is higher for the Incoloy than the Inconel and MP35N, whereas Mo and Ni segregation is less for the Incoloy. The extent of Mo segregation appears to vary in accordance with the Ni content of the alloy.

- The film on Inconel 718 is basically a Ni-Cr-Fe type with a small amount of Mo, whereas the film on Incoloy 925 is considered a Ni-Cr-Fe-Cu oxide. In the case of MP35N, the film is principally a Ni-Cr-Co type, but it contains more Mo than the other two alloys.

- The high Cr content of the oxides accounts in large part for the high corrosion resistance of these alloys, and MP35N in particular further benefits from a relatively high level of Mo in the film. The smaller amounts of Mo in the oxides on the Inconel and Incoloy are compensated for, to some extent, by enriched levels of Nb and Cu, respectively.

- The thickness of the films is similar for the three alloys and is estimated at 1.5 ± 0.5 nm. These films are thin enough that they represent a negligible fraction of the total diffusion distance traversed by hydrogen during charging times of 10 s and longer.

REFERENCES

1. S. P. Clough and T. R. Pinchback, J. Mater. Energy Syst. **1**, 55 (1979).

2. W. F. Bogaerts, A. A. Van Haute, and M. J. Brabers, in *Proceedings of the International Congress on Metallic Corrosion*, Toronto, Canada (1984), Vol. 2, p. 388.

3. C. H. Becker and K. T. Gillen, Anal. Chem. **56**, 1671 (1984).

4. J. B. Pallix, C. H. Becker, and N. Newman, Mater. Res. Bull. **12** (6), 52 (1987).

5. D. D. Macdonald, M. Ben-Haim, and J. Pallix, J. Electrochem. Soc. **136**, 3269 (1989).

6. C. H. Becker and K. T. Gillen, J. Vac. Sci. Technol. **A3**, 1347 (1985).

7. C. H. Becker in *Ion Spectroscopies of Surfaces*, eds. A. W. Czanderna and D. M. Hercules (Plenum, New York, 1990) in press.

8. C. H. Becker and K. T. Gillen, J. Opt. Soc. Am. **B2**, 1438 (1985)

9. C. H. Becker, J. Vac. Sci. Technol. **A5**, 1181 (1987).

10. *Sputtering by Particle Bombardment*, Vol. 1, R. Behrisch, ed. (Springer, New York, 1981).

11. J. B. Lumsden and R. W. Staehle, Scr. Metall. **6**, 1205 (1972).

12. K. Sugimoto and S. Matsuda, Mater. Sci. Eng. **42**, 181 (1980).

13. A. Schneider, D. Kuron, S. Hofmann, and R. Kirchheim, Corros. Sci. **31**, 191 (1990).

14. C. E. Locke, J. H. Peavey, O. Rincon, and M. Afzal, in Proc. Symp. Adv. in Characterization of Metal and Polymer Surfaces, L-H. Lee, ed. (New York, 1976; Academic Press, New York, 1977), Vol. 1, p. 155.

15. G. Okamoto and T. Shibata, in Proc. 4th Int. Symp. Passivity, R. P. Frankenthal and J. Kruger, eds. (Electrochem. Society, Princeton, New Jersey, 1978), p. 646.

16. G. J. Barnes, A. W. Aldag, and R. C. Jerner, J. Electrochem. Soc. **119**, 684 (1972).

17. A.E. Yaniv, J. B. Lumsden, and R. W. Staehle, in *Passivity and its Breakdown on Iron and Iron-Base Alloys*, U.S.A.-Japan Seminar, R. W. Staehle and H. Okuda, eds. (NACE, Houston, Texas, 1962), p. 72; J. Electrochem. Soc. **124**, 490 (1977).

18. K. Teramoto, K. Asami, K. Hashimoto, and S. Shimodaira, Preprints of 76th Spring Meeting of Japanese Institute of Metals (Tokyo, 1975), p. 96; Extended

Abstracts of Spring Meeting of Japanese Society of Corrosion Engineers (1976), p. 4.

19. J. P. Stroup, A. H. Bauman, and A. Simkovich, Mater. Perform. **15**, 43 (1976).

20. M. Seo, G. Hultquist, C. Leygraf, and N. Sato, Corros. Sci. **26**, 949 (1986).

21. N. Tomashov, Corrosion **14**, 299t (1958).

22. B. G. Pound, Corrosion **46**, 50 (1990).